DIELECTRIC PROPERTIES OF SNOW IN THE 3- TO 37-GHz RANGE

Martti Hallikainen, Fawwaz T. Ulaby, and M. Abdelrazik

Abstract

Microwave dielectric measurements of dry and wet snow were made at nine frequencies between 3 GHz and 18 GHz, and at 37 GHz, using two free-space transmission systems. The measurements were conducted during the winters of 1982 and 1983. The following parametric ranges were covered: (a) liquid water content, 0 to 12.3% by volume; (b) snow density, 0.09 to 0.42 g • cm^{-3}; (c) temperature, 0 to -5°C and -15°C (scattering-loss measurements); and (d) crystal size, 0.5 to 1.5 mm. The experimental data indicate that the dielectric behavior of wet snow closely follows the dispersion behavior of water. For dry snow, volume scattering is the dominant loss mechanism at 37 GHz. The applicability of several empirical and theoretical mixing models was evaluated using the experimental data. Both the Debye-like semiempirical model and the theoretical Polder-Van Santen mixing model were found to describe adequately the dielectric behavior of snow. However, the Polder-Van Santen model provided a good fit to the measured values of the real and imaginary parts of wet snow only when the shapes of the water inclusions in snow were assumed to be both nonsymmetrical and dependent upon snow water content. The shape variation predicted by the model is consistent with the variation suggested by the physical mechanisms governing the distribution of liquid water in wet snow.

This work was supported by the Army Research Office under Grant DAAG29-81-K-0142.

M. Hallikainen is with the Helsinki University of Technology, Otaniemi, Finland.

F. T. Ulaby is with the Radiation Laboratory, Dept. of Electrical Engineering and Computer Science, University of Michigan, Ann Arbor, MI 48109.

M. Abdelrazik is with E-Systems, Greenville, TX 75401.

I. INTRODUCTION

Dry snow is a mixture of ice particles and air voids. After a snowfall, the shapes of the numerous ice particles in dry snow are modified by metamorphism. Thermodynamically, the ice crystals seek equilibrium, for which the ratio of surface area to volume is minimum [1]. Any water in the snowpack collects at points of contact between the grains. The geometry and porosity of snow at high and low liquid water contents have been examined by Colbeck [2]. He concluded that snow, like any porous material, has two distinct regimes of liquid saturation. In the lower range, called the pendular regime, air is continuous throughout the pore space, and liquid occurs in the form of isolated inclusions. In the higher range of liquid saturation, the funicular regime, the liquid is continuous throughout the pore space and air occurs as distinct bubbles trapped by narrow constrictions in the pores. There is a sharp transition between the two regimes.

The metamorphism caused by melting and freezing changes the microstructure of snow; the grains become rounded during the melting process, and some of the smaller grains disappear completely. Snow that has undergone several melt-freeze cycles tends to form multiple clusters.

In general, a snow medium is electromagnetically a three-component dielectric mixture consisting of air, ice particles, and liquid water. Both ice and water exhibit dispersion spectra; however, the relaxation frequency of ice is in the kilohertz range, whereas that for water at 0°C is about 9 GHz [3]. The complex dielectric constants of ice (a low-loss material) and water (a high-loss material) depend on frequency and temperature. Consequently, the dielectric constant of snow, in general, is

a function of frequency, temperature, volumetric water content, snow density, ice-particle shape, and the shape of the water inclusions.

Over the last few years, several investigations have been conducted to evaluate the use of microwave remote sensing systems in determining the extent, water equivalent, and liquid water content of snow cover. Passive measurements of snowpacks have been made in the 5- to 94-GHz range [4]-[7], and active measurements have been reported for frequencies between 1 GHz and 36 GHz [5], [8]. The measurements include data for both dry and wet snow conditions. Radiometric observations provided by Nimbus-7 at 18 GHz and 37 GHz have been employed in snow studies on both a global and a regional scale [9], [10].

These studies indicate that the frequency range of both active and passive remote-sensing measurements and the utilization of the data available have been extended to millimeter wavelengths. However, the basic tool used to interpret these data, namely the microwave dielectric properties of snow, are known with satisfactory accuracy only for frequencies below 13 GHz. In fact, as is shown in Table 1, only a few microwave dielectric measurements of snow have been made to date. They include only two multifrequency investigations: a study of wet snow between 4 GHz and 12 GHz [14], and one for dry snow at four frequencies between 0.8 GHz and 13 GHz [15]. Linlor's sample preparation technique involved mixing liquid water at 0°C with dry snow [14], which caused the water distribution in the mixture to be different from that found in natural snow.

The extent to which the microwave properties of snow can be modeled is naturally limited to the frequency ranges of reported experimental studies. Mixing models that assume wet snow to consist of either dry snow

and water or, more fundamentally, of air, ice, and water, have been applied by several investigators [11], [16]-[19]. Because of the lack of wideband dielectric data for natural snow, the capability of these models to satisfactorily describe the microwave dielectric behavior of dry and wet snow is still an open question.

This study presents the results of dielectric measurements made over the 3- to 18-GHz range, and at 37 GHz, for natural (dry and wet) snow. Several empirical and theoretical models were applied to fit the experimental data. In addition, a study of scattering losses in dry and wet snow is included.

II. LOSSES IN AN INHOMOGENEOUS MEDIUM

An inhomogeneous material is said to have an effective or equivalent dielectric constant ε defined such that a wave propagating in an equivalent homogeneous material with dielectric constant ε would experience the same attenuation rate and phase delay as the wave does in the real (inhomogeneous) material. If the inclusions in the inhomogeneous medium are much smaller than the wavelength and if their shapes are known, it is possible to relate ε, the dielectric constant of the mixture, to the dielectric constants of the consistent (inclusions and host) materials. These relations, known as dielectric mixing models, are the subject of numerous articles, some of which are referred to in later sections in this paper. An important assumption underlying all of these models is that scattering losses in the medium may be neglected because they are much smaller than absorption losses. We shall now examine the situation for dry and wet snow.

A. Dry Snow

Dry snow is an inhomogeneous medium consisting of ice crystals in an air background. If we assume the ice particles to be spherical, we can use Mie expressions to compute the absorption, scattering, and extinction cross-sections of each particle in terms of the particle radius r and the relative dielectric constant ε_i [3, pages 290-294]. If, in addition, we assume that all the ice particles are identical and ignore mutual interaction between them, we can easily compute the absorption, scattering and extinction coefficients of the snow medium, κ_a, κ_s, and κ_e, respectively, by summing over the number of particles per unit volume. The curves in Fig. 1 are the result of such a computation. They indicate that for snow consisting of 1-mm diameter ice crystals, absorption and scattering losses are about equal at 14 GHz, absorption losses dominate at lower frequencies and scattering losses dominate at higher frequencies. For snow with larger crystals, the intersection point of the curves representing κ_a and κ_s (at which the scattering albedo $\alpha = \kappa_s/(\kappa_s + \kappa_a) = 0.5$) would occur at a frequency lower than 14 GHz. These results lead to the conclusion that the concept of equivalent dielectric constant is inapplicable to dry snow over most of the microwave region. A closer look, however, reveals that it is indeed possible to define an equivalent prmittivity ε'_{ds} for dry snow because the dielectric loss tangent of ice, $\tan \delta_i = \varepsilon''_i/\varepsilon'_i$, is much smaller than unity. The phase velocity in dry snow is essentially a function of only ε'_i and the snow density ρ_s and independent of ε''_i. Thus, an equivalent permittivity ε'_{ds} may be defined for dry snow from measurements of phase constant β, regardless of the magnitude of the scattering albedo of the dry-snow medium.

B. Wet Snow

Wet snow is assumed to consist of ice spheres imbedded in an air-water mixture (wet-air background). The absorption coefficient is given by

$$\kappa_a = \kappa_{ai} + \kappa_{ab} \tag{1}$$

where κ_{ai} is the absorption coefficient due to the ice spheres and κ_{ab} is due to the background. Detailed expressons for calculating κ_{ai}, κ_{ab}, and the scattering coefficient κ_s are given in Eom et al. [32]. Figure 2 shows plots of the scattering albedo as a function of the snow liquid water content m_v. Calculations made at several frequencies between 1 and 40 GHz show that $\kappa_{ai} << \kappa_{ab}$ if $m_v > 1\%$. Furthermore, if (a) κ_s is ignored in favor of κ_a, (b) loss measurements are assumed to be entirely due to absorption, and (c) wet snow is treated as an equivalent homogeneous medium with dielectric constant ε_{ws}, the values of ε'_{ws} and ε''_{ws} estimated from the loss measurements would be in error by less than 1% and 2%, respectively, if $m_v > 1\%$ for $f < 18$ GHz. At 37 GHz, the errors are less than 1% for ε'_{ws} and 10% for ε''_{ws} if $m_v > 2\%$.

In the calculations leading to the above conclusions, the liquid water is treated as randomly oriented spheroids with constant depolarization factors. As we will see later, the results of this investigation indicate that the depolarization factors, which are related to the shape of the water ellipsoid, exhibit a definite dependence on m_v. Nonetheless, the calculations provide reasonable estimates for evaluating the conditions of applicability of the experimental data reported in this study.

III. MEASUREMENT TECHNIQUES

Two free-space transmission systems, one operating between 3 GHz and 18 GHz [20] and the other operating at 37 GHz [21], were used in the snow dielectric measurements. The free-space technique is practical for producing data over a wide frequency range, because the same sample can be measured over the entire range. In addition, the free-space technique allows the rapid measurement of wet snow samples, which assures that their properties are accurately represented. During the measurement process, the two free-space systems were placed in an unheated truck. The temperature inside the truck was 0 ± 2°C during the measurement of wet snow samples and well below 0°C when dry snow samples were measured.

A. Free-Space Transmission Technique

3- to 18-GHz System

Figure 3a is a block diagram of the 3- to 18-GHz system. The antenna separation is 23 cm and the sample diameter is 30 cm. Two methods were used to account for multiple reflections within the measurement system: (1) a pulley system to move the sample between the horn antennas during the phase-shift measurements, and (2) swept-frequency loss measurements to record and average the reflections. The maximum loss measurable by the system is 40 dB.

The complex transmission coefficient for a sample was measured by comparing the amplitude and phase readings of the network analyzer/phase-gain indicator for the sample holder when empty and when filled with snow.

$$T_m = |T_m| \, e^{j\phi_m} = \frac{(1 - R^2) \, e^{-\gamma d}}{1 - R^2 \, e^{-2\gamma d}} , \qquad (2)$$

where γ is the complex propagation constant for the sample, defined in terms of the attenuation coefficient α and the phase coefficient β as

$$\gamma = \alpha + j\beta ,$$

where

$$\alpha = \frac{2\pi}{\lambda_0} \left[\sqrt{\frac{\varepsilon'}{2}} \left(\left[\sqrt{1 + \left(\frac{\varepsilon''}{\varepsilon'}\right)^2} \right]^{1/2} - 1 \right) \right]^{1/2} \tag{3}$$

$$\beta = \frac{2\pi}{\lambda_0} \left[\sqrt{\frac{\varepsilon'}{2}} \left(\left[\sqrt{1 + \left(\frac{\varepsilon''}{\varepsilon'}\right)^2} \right]^{1/2} + 1 \right) \right]^{1/2} . \tag{4}$$

The electric-field reflection coefficient is denoted by R and the sample thickness by d. The complex dielectric constant of the sample is $\varepsilon = \varepsilon' - j\varepsilon''$.

The expressions for the magnitude $|T_m|$ and the phase ϕ_m of the transmission coefficient T_m are coupled nonlinear functions of α and β, and hence of ε' and ε''. Therefore, an iterative procedure was used to obtain ε' and ε'' [20].

37-GHz System

A block diagram of the measurement system is shown in Figure 3b. The antenna separation is 37 cm, and the sample diameter is 30 cm (same sample as for the 3- to 18-GHz system). The measurement procedure for this system is different from that for the 3- to 18-GHz system. During the loss measurement, the reference arm was blocked out by a variable attenuator.

The sample loss was obtained by measuring the transmitted power, both with and without the sample inserted. A frequency sweep from 37 GHz to 38 GHz was employed to record and then eliminate multiple reflections. The maximum loss measurable by the present 37-GHz system is 40 dB.

Instead of measuring the phase shift due to the sample at a fixed frequency, the interference pattern between 37 GHz and 38 GHz was recorded. The interference is a result of splitting the signal between the reference arm and the test arm and then recombining it. Due to the phase shift from the sample, the frequency maximum of the interference patterns without the sample, f_1, and with the sample inserted, f_2, were observed.

The real part of $\sqrt{\varepsilon}$ can be computed from those frequencies and from the geometry of the measurement system [21]

$$\mathrm{Re}\{\sqrt{\varepsilon}\} = 1 + \frac{\lambda_{02}}{d}\left[l_r\left(\frac{1}{\lambda_{r2}} - \frac{1}{\lambda_{r1}}\right) - l_t\left(\frac{1}{\lambda_{t2}} - \frac{1}{\lambda_{t1}}\right)\right] - \frac{s}{d}\left(\mathrm{Re}\sqrt{\varepsilon_s} - 1\right) . \tag{5}$$

In (5), l_r and l_t are the lengths of the reference arm and the test arm, respectively, d is the sample thickness, and λ_i refers to wavelength at frequency f_i ($i = 1$ or 2). The subscript r refers to the reference arm (waveguide) and t to the test arm (free space). The thickness and the complex dielectric constant of the sample holder are designated s and ε_s, respectively. From the measured values for loss L ($L = |T_m|$) and $\mathrm{Re}\{\sqrt{\varepsilon}\}$, ε' and ε'' can be computed using an iteration process as described in [21].

B. Measurement Accuracy and Precision

Measurement accuracy depends upon the measurement technique used and upon the dielectric properties and dimensions of the sample. For wet snow samples, the preservation of the sample's properties (especially its liquid water content) during the measurement is important.

3- to 18-GHz System

In order to determine the absolute precision of the system, test samples ranging from low-loss material (polymethyl methacrylate) to high-loss material (distilled water) were measured [20]. The average deviation from previously observed values over the 3- to 18-GHz range for polymethyl methacrylate (ε = 2.60 - j0.015 at 3 GHz, ε = 2.57 - j0.0082 at 25 GHz [22]) was 1.2% for ε' and 0.02 dB for the loss; for distilled water (ε = 77.1 - j11.6 at 3 GHz, ε = 43.2 - j33.0 at 18 GHz for T = 23°C [3]), the deviation was 2.1% for ε' and 2.8% for ε''. The 3- to 18-GHz system is not sufficiently accurate to measure the loss from the dry snow samples.

The total calculated worst-case error bounds for the measurement of wet snow samples is shown in Fig. 4. The samples represent an upper limit (m_v = 12%), a lower limit (m_v = 1.6%), and a median value (m_v = 5.6%) for snow-sample liquid water content by volume, in this study. The thickness of the sample was increased with decreasing water content in order to increase the sample loss and, consequently, to increase the accuracy of the measurement. These error bounds include the uncertainties both in the free-space transmission system and in the interpretation of the measurements.

The 3- to 18-GHz free-space system was tested against a 4- to 6-GHz waveguide transmission system at 6 GHz, using loamy soil samples. The results show good agreement between the two systems [20].

37-GHz System

The 37-GHz system was tested using the same test material used for the 3- to 18-GHz system. For polymethyl methacrylate ($\varepsilon = 2.57 - j0.0082$ at 25 GHz [22]), the deviation from previously reported values was 1.5% for ε' and 25% for ε'', whereas for distilled water ($\varepsilon = 19.6 - j29.5$ at 37.5 GHz [3]), the corresponding value was 1.0% for both ε' and ε''. The increase in the accuracy of ε'' is due to the high loss ($L > 30$ dB) of the water sample compared with that of the polymethyl methacrylate sample ($L = 1$ dB).

The total error bounds for the measurement of wet snow samples were calculated, taking into consideration the uncertainties in both the measurement system and the reading accuracy. For water contents of $m_v \geq 5.6\%$, the worst-case error bounds for ε' and ε'' are 4% and 5%, respectively. For $m_v = 1.6\%$, they are 4% and 8%, respectively.

C. Sample Preparation

The snow samples were acquired in an open area, from various depths in the snow cover, including the bottom and top layers. Two styrofoam sample holders were used, one for dry snow and the other for wet snow. Each holder was 30 cm in diameter and tray-like in shape. The dry-snow holder was 10 cm deep, whereas the wet-snow holder was configured to be only 2 cm deep because of the much higher loss typical of wet snow. Extreme care was taken not to disturb the structure of the samples: the extra snow around a potential sample was removed, and the sample holder was placed upside down

on top of the sample; the sample was then cut, turned right-side up, and its surface was smoothed with a straightedge.

Upon completion of the microwave dielectric measurements using the 3- to 18-GHz and the 37-GHz free-space systems, the holder containing the snow sample was weighed and the thickness of the sample was measured. The temperature of the sample was measured using a temperature probe and digital multimeter. A freezing-calorimeter was used to measure the snow's liquid water content. Immediately following this step, the parameters of the snow-crystals were observed, using a microscope with a fiber-optic light source to minimize any heating effects. After each new snowfall, the pH level of the snow samples was examined, i.e., a small sample of snow was allowed to melt, and its pH value was then measured using a pH-meter.

In order to obtain the density of dry snow from the measured density of a wet snow sample, the following expression (used by Ambach and Denoth [23]) was used in this study:

$$\rho_{ds} = \frac{\rho_{ws} - m_v}{1.0 - m_v}, \tag{6}$$

where ρ_{ds} is the density of dry snow in g cm^{-3}, ρ_{ws} is the density of wet snow in g cm^{-3}, and m_v is the volume fraction of liquid water (the volumetric water content) within the snow sample.

During the 1982 experiment, the snow samples were not insulated at the upper surface; as a result, the snow's liquid water content varied with time during the measurement. In order to find the actual water content as a function of time, the first and last measurement of each sample was made at 18 GHz. This allowed the calorimetrically measured water content value

to be corrected. In 1983, however, the samples were insulated with styrofoam and no corrections were needed.

IV. EXPERIMENTAL DATA

A comprehensive data base for the complex dielectric constant of snow between 3 GHz and 37 GHz was established in 1982 and 1983. In 1982, measurements were conducted at nine equally spaced frequencies between 4 GHz and 18 GHz. In 1983, two frequencies were added, resulting in a frequency range of 3 to 37 GHz.

The data base for the snow dielectric measurements consisted of 995 data points, 584 of which were for wet snow and 411 for dry snow. The number of snow samples measured at each frequency between 4 GHz and 18 GHz (using 2-GHz intervals) was about 110, whereas 63 samples were measured at 3 GHz and at 37 GHz. The snow samples had densities ranging from 0.09 g cm^{-3} to 0.42 g cm^{-3} and liquid water contents ranging between 0% and 12.3% by volume. The snow-particle size varied between 0.5 mm and 1.5 mm, and the pH level ranged from 5.6 to 6.5. Sample temperatures ranged from -5°C to 0°C. All snow samples consisted of fairly new snow. Two examples of the experimental data are given in Fig. 5. The results of the 1983 measurements agree well with those obtained in 1982.

In addition, the loss from several dry snow types was measured at 37 GHz, where volume scattering is the dominant loss mechanism. For each snow type, different thicknesses were used in order to increase the accuracy of the measurement. Prior to measurement, some of the samples were stored for one year in a freezer. The density of the samples ranged from 0.32 g cm^{-3} (new snow) to 0.43 g cm^{-3} (refrozen snow) and the grain

size from 1.0 mm to 1.5 mm, correspondingly. The temperature of the samples was -15°C.

V. DIELECTRIC MODELS

The experimental data were used to develop and evaluate several theoretical and empirical snow dielectric models. The evaluation of the models was performed using the residual sum of squares, given by

$$RSS = \sum_{i=1}^{n} [\varepsilon_i(obs) - \varepsilon_i(pred)]^2 , \tag{7}$$

where $\varepsilon_i(obs)$ is the measured value, $\varepsilon_i(pred)$ is the estimated value calculated from the model, and n is the number of data points. Equation (7) was used separately for ε' and ε''.

The rms error for ε' is

$$e'_{rms} = \left[\frac{RSS}{n} \right]^{1/2} , \tag{8}$$

and a similar expression applies to ε''.

The square of the correlation coefficient, r^2, measures the proportion of the total variation about the mean value explained by the regression.

As a third criterion, linear regressions of the form

$$\varepsilon'(obs) = \alpha'\varepsilon'(pred) + \beta' \tag{9}$$

$$\varepsilon''(obs) = \alpha''\varepsilon''(pred) + \beta'' \tag{10}$$

were used to evaluate the models. A perfect model is one for which $\alpha' = \alpha'' = 1$ and $\beta' = \beta'' = 0$, and for which the linear regression coefficients for ε'_{ws} and ε''_{ws} are close to unity in magnitude.

A. Dry Snow

Dry snow is a mixture of ice and air. The permittivity of ice is independent of temperature and frequency at microwave frequencies [24], which causes the permittivity of dry snow ε'_{ds} to be independent of temperature and frequency as well. The acquired data for ε'_{ds} in the 3- to 37-GHz range, shown in Fig. 6, were found to follow a linear density dependence, given by

$$\varepsilon'_{ds} = 1.8317\ \rho_{ds} \ ; \quad 0.09 \leq \rho_{ds} \leq 0.40 \text{ g cm}^{-3} \ . \tag{11}$$

The estimate of the rms error between the measured values and those predicted by (11) is 0.038, However, (11) tends to overestimate the values of ε'_{ds} for low snow densities and underestimate them for high snow densities. By combining the present data with previous experimental values [11], [15], [25], two expressions were derived for ε'_{ds}:

$$\varepsilon'_{ds} = 1 + 1.9\ \rho_{ds} \ ; \quad \rho_{ds} \leq 0.5 \text{ g cm}^{-3} \tag{12a}$$

$$\varepsilon'_{ds} = 0.51 + 2.88\ \rho_{ds} \ ; \quad \rho_{ds} \geq 0.5 \text{ g cm}^{-3} \ . \tag{12b}$$

Plots of the above expressins are shown in Fig. 7.

Expressions similar to (11) have been reported in the literature for frequencies below 13 GHz with slightly larger values for the coefficient of ρ_{ds} [23], [26]. The larger values are due to the higher range of density of the tested snow samples. In this paper, Eq. (11) will be used to describe the dependence of ε'_{ds} on snow density.

The imaginary part (or loss factor) of the dielectric constant of dry snow, ε''_{ds}, is of the order of 10^{-3} in the microwave region, and is therefore difficult to measure with accuracy. The cavity technique is needed to measure the dielectric properties of materials with very low losses. The measurements of ε''_{ds} made with the free-space transmission system are not accurate enough to use for model evaluations. From the theoretical Polder-Van Santen mixing model [27], however, the following formula may be obtained by assuming the ice particles to be spherical:

$$\varepsilon''_{ds} = \frac{0.34\ v_i \varepsilon''_i}{(1 - 0.417\ v_i)^2}\ , \tag{13}$$

where $v_i = \rho_{ds}/\rho_i$ is the ice volume fraction, $\rho_i = 0.916$ g cm^{-3} is the density of ice, and ε''_i is the loss factor of ice. Figure 8 shows that $\varepsilon_{ds}/\varepsilon''_i$ from (13) agrees well with Cumming's data for dry snow over a wide range of snow densities. The dependence of ε''_i on frequency and temperature was examined by Nyfors [15] and by Stiles and Ulaby [28].

B. Wet Snow

Six dielectric mixing models were considered, including (a) the two-phase Polder-Van Santen model [27] (dry-snow-plus-water mixture), (b) the three-phase Polder-Van Santen model (ice, air, and water), (c) the confocal ellipsoidal model [29], (d) the refractive model [31], (e) an empirical model based on Linlor's formulation [14], and (f) the Debye-like semiempirical model described below. Of these, only models (a), (b), and (f) provided results in good agreement with experimental observations.

In the theoretical models, wet snow is assumed to consist of either dry snow (with $\varepsilon_{ds} = \varepsilon'_{ds} - j\varepsilon''_{ds}$) and water (with $\varepsilon_w = \varepsilon'_w - \varepsilon''_w$), or of air

(with $\varepsilon_a = 1$), ice (with $\varepsilon_i = \varepsilon_i' - j\varepsilon_i''$), and water. For dry snow, ε_{ds}' is calculated from Eq. (11), and ε_{ds}'' is calculated from (13); for water, ε_w is calculated from the Debye equation [3]; and for ice, $\varepsilon_i' = 3.15$ [24], and ε_i'' is calculated using the results reported in [15].

Two-Phase Polder-Van Santen Model

The complex dielectric constant of wet snow, $\varepsilon_{ws} = \varepsilon_{ws}' = j\varepsilon_{ws}''$, is assumed to be a mixture of dry snow (host) and liquid water (inclusions). The water droplets are randomly distributed and randomly oriented ellipsoids with depolarization factors A_{w1}, A_{w2}, and A_{w3}. The mixing formula is given by

$$\varepsilon_{ws} = \varepsilon_{ds} + \frac{m_v \varepsilon_{ws}}{3} (\varepsilon_w - \varepsilon_{ds}) \sum_{j=1}^{n} [\varepsilon_{ws} + (\varepsilon_w - \varepsilon_{ws}) A_{wj}]^{-1} , \qquad (14)$$

where m_v is the liquid water content (volume fraction of water).

In previous efforts to model wet snow using the two-phase Polder-Van Santen mixing model, the water inclusions were assumed to be symmetrical in shape, that is, $A_{w1} = A_{w2}$, and $A_{w3} = 1 - 2A_{w1}$ [18]. On the other hand, hydrologic models indicate that the shape of the water inclusions may vary as a function of water content. Ambach and Denoth [18] fitted their experimental data for ε_{ws}' (below 1 GHz) using the symmetrical approach. They observed that the optimum value of A_{w1} varied between 0.01 and 0.08, generally increasing with increasing water content.

In the present investigation, three approaches were taken when applying the two-phase Polder-Van Santen mixing model: (a) the water

inclusions were assumed to be symmetrical ($A_{w1} = A_{w2}$, $A_{w3} = 1 - 2A_{w1}$), and the shape of the inclusions was assumed to be independent of snow water content; (b) the water inclusions were assumed to be nonsymmetrical ($A_{w1} \neq A_{w2} \neq A_{w3}$) and their shape to be independent of snow water content; and (c) the water inclusions were assumed to be nonsymmetrical and their shape was assumed to depend upon snow water content. In each case, optimum values for A_{wi} were sought by minimizing the error between the values of ε_{wa} as calculated from (14) and those obtained experimentally.

Table 2 shows the results of the optimization processes. The symmetrical approach gave $A_{w1} = 0.074$ when the optimization was performed using ε''_{ws} data. However, the corresponding value using ε'_{ws} data was $A_{w1} = 0.155$. The fact that different depolarization factors are needed to describe the behavior of ε'_{ws} and ε''_{ws} renders the symmetrical approach unacceptable and suggests that the water inclusions are not symmetrical.

The second approach, in which the water inclusions were assumed to be nonsymmetrical in shape and to retain this shape independently of snow water content, gave $A_{w1} = 0.067$ and $A_{w2} = 0.251$, when the optimization was performed using ε''_{ws} data. The superiority of the nonsymmetrical approach compared to the symmetrical one is indicated by the fact that the same set of values of A_{wi} (optimized using ε''_{ws} data) gives a reasonably good fit to ε'_{ws} as well.

Finally, A_{w1}, A_{w2}, and A_{w3} were optimized separately as a function of water content using ε''_{ws} data. Each water-content category was $\Delta m_v = 1\%$ in range, that is, $0.0 \leq m_{v1} < 1.0\% \leq m_{v2} < 2.0\%$, etc., and the last region was $11.0 \leq m_{v12} < 12.5\%$. The optimized depolarization factors are shown in Fig. 9 as a function of liquid water content. According to these results, the water inclusions in snow appear needle-like in shape ($A_{w1} = 0.0$, $A_{w2} =$

A_{w3} = 0.5 for perfect needles) for liquid water contents below m_v = 3%. However, they become disc-like for $m_v \geq 3\%$ ($A_{w1} = A_{w2} = 0.0$, $A_{w3} = 1.0$ for discs). This change in shape appears to be due to the transition from the pendular regime to the funicular regime. The transition value is slightly lower than that calculated by Colbeck [17]; this is attributed to the lower range of density values of the snow samples examined in the present study.

The two-phase Polder-Van Santen model with nonsymmetrical water inclusions (whose shape depends on snow water content) is found to be in excellent agreement with the measured ε''_{ws} data, as shown in Table 2. The depolarization factors optimized previously, using the measured values of ε''_{ws} as a function of m_v, can be used in the two-phase Polder-Van Santen mixing model to estimate the values of ε'_{ws}. Table 2 shows the statistics of the predicted ε'_{ws} values as compared to the measured values. The model works well at all frequencies.

Three-Phase Polder-Van Santen Model

Instead of treating wet snow as a two-phase mixture consisting of dry snow and liquid water, the three-phase mixing model treats it as a mixture of air (host), ice, and liquid water. The expression for ε_{ws} is fundamentally similar to that given in (14), except that it contains two summations: one over the depolarization factors of the ice inclusions (which are assumed to be spherical) and another over the depolarization factors of water:

$$\varepsilon_{ws} = 1 + \frac{1}{3}\varepsilon_{ws} v_i(\varepsilon_i - 1) \sum_{j=1}^{3} [\varepsilon_{ws} + (\varepsilon_i - \varepsilon_{ws}) A_{ij}]^{-1}$$

$$+ \frac{1}{3}\varepsilon_{ws} m_v(\varepsilon_w - 1) \sum_{j=1}^{3} [\varepsilon_{ws} + (\varepsilon_w - \varepsilon_{ws}) A_{wj}]^{-1} . \qquad (15)$$

In (15), m_v is the volume fraction of water (the liquid water content), and A_{wj} and A_{ij} are the depolarization factors of the water and ice inclusions, respectively, with $A_{ij} = 1/3$. Again, the three approaches concerning the depolarization factors of the water inclusions were used.

The symmetrical approach yielded results close to those obtained using the corresponding two-phase Polder-Van Santen model, which suggest, again, that the water inclusions in snow are not symmetrical. The best agreement with the measured ε''_{ws} and ε'_{ws} data is again obtained by assuming that the water inclusions are nonsymmetrical in shape and that their shape depends on snow water content. In fact, the optimized values of A_{wi}, obtained with the three-phase model are very close to those shown in Fig. 9 which belong to the two-phase model. the rms errors also are approximately equal for the two models (Table 3). Considering its simpler formulation, the two-phase model is preferred from a computational standpoint.

Debye-Like Model

The dielectric constant of dry snow is of the order of $\varepsilon_{ds} \simeq 1.6 - j10^{-3}$. The water inclusions have an ε'_w about 40 times larger than ε'_{ds}. Hence, even when the liquid water content is of the order of only 1 percent by volume, the spectral behavior of the wet snow mixture is likely to be dominated by the dispersion behavior of water. This argument led to the testing of the following semiempirical model:

$$\varepsilon'_{ws} = A + \frac{B\, m_v^X}{1 + (f/f_0)^2} \tag{16}$$

$$\varepsilon''_{ws} = \frac{C(f/f_0)\, m_v^X}{1 + (f/f_0)^2} \tag{17}$$

where f_0 is the relaxation frequency, f is the frequency, and A, B, C, and x are all constants to be determined by fitting the model to the measured data in the 3- to 37-GHz range. Such an approach gives

$$A = 1.0 + 1.83\ \rho_{ds} + 0.02\ A_1\ m_v^{1.015} + B_1 \tag{18a}$$

$$B = 0.073\ A_1 \tag{18b}$$

$$C = 0.073\ A_2 \tag{18c}$$

$$x = 1.31 \tag{18d}$$

$$f_0 = 9.07\ \text{GHz} \tag{18e}$$

$A_1 = A_2 = 1.0$ and $B_1 = 0$ for Debye-like model

(expressions given below for modified Debye-like model)

The value of f_0 is slightly higher than the relaxation frequency of water at 0°C, $f_{0w} = 8.8$ GHz [3]. This is in agreement with the results of previous studies concerning heterogeneous mixtures containing water. Both theoretically and experimentally, de Loor has found that the relaxation frequency of such mixtures is always equal to or higher than that of the relaxing component [30]. In addition, he concluded that the closer the relaxation frequency of the mixture is to the relaxation frequency of the inclusions, the greater the departure of the shape (i.e., approaching disc- or needle-like forms) from the spherical will be. Therefore, the optimized nonsymmetrical approach adopted in the previous sections for determining A_{wi} is in concert with the value of the relaxation frequency in (18e).

Table 3 provides a comparison of the rms errors associated with the Debye-like model with those of the Polder-Van Santen models. The Debye-like model is simpler to use, but its accuracy is poorer above 15 GHz.

Modified Debye-Like Model

The accuracy of the Debye-like model may be improved, however, by expressing the constants A, B, and C in (18) in terms of the following empirically determined functions:

$$A_1 = 0.78 + 0.03\ f - 0.58 \times 10^{-3}\ f^2 \tag{19a}$$

$$A_2 = 0.97 - 0.39\ f \times 10^{-2} + 0.39 \times 10^{-3}\ f^2 \tag{19b}$$

$$B_1 = 0.31 - 0.05\ f + 0.87 \times 10^{-3}\ f^2, \tag{19c}$$

where f is in GHz. This will be referred to as the modified Debye-like model. the importance of the frequency dependent constants is primarily at frequencies above 15 GHz; below 15 GHz, we may set $A_1 = A_2 = 1.0$ and $B_1 = 0$.

VI. EVALUATION OF THE DIELECTRIC MODELS

It was noted earlier that the permittivity of dry snow is a funcion of density only. In order to examine the variation of the permittivity of wet snow ε'_{ws} with liquid water content m_v, it is useful to define the incremental permittivity $\Delta\varepsilon'_{ws}$,

$$\Delta\varepsilon'_{ws} = \varepsilon'_{ws} - \varepsilon'_{ds}$$

$$= \varepsilon'_{ws} - 1 - 1.8317\ \rho_{ds} \tag{20}$$

which, as we will see, is approximately independent of density. Thus, $\Delta\varepsilon'_{ws}$ is the contribution due to liquid water. For ε''_{ws}, no incremental quantity is needed because liquid water dominates the loss factor.

Figure 10 shows the measured permittivity and the dielectric loss factor at 6 GHz as a function of liquid water content. The solid curves were calculated using the Debye-like model. As indicated by these figures, the fit is quite good. Similar fits were also obtained with the Polder-Van Santen models. The difference in behavior between the Debye-like and the Polder-Van Santen models is significant only at frequencies above 15 GHz; Fig. 11 provides a comparison of the two types of models against the data at 37 GHz. The overall fit of the two-phase Polder-Van Santen model to the data is shown in the form of scatter plots in Fig. 12.

Figures 13 to 15 show the effect of liquid water content on the dielectric behavior of wet snow between 3 GHz and 37 GHz. The results are shown for a dry snow density ρ_{ds} = 0.24 g cm^{-3}, which was the average observed value during this study. The values of ε'_{ws} and ε''_{ws} were calculated using the modified Debye-like equations (16) - (19). As shown in Figs. 13 to 15, ε''_{ws} reaches its maximum value at 9.0 GHz. This agrees with the relaxation frequency of water at 0°C. The sharp increase in ε''_{ws} between 3 GHz and 6 GHz is due to the large increase in the magnitude of ε''_{w} for water over this frequency range. The attenuation constant of wet snow increases practically linearly with frequency up to 15 GHz. Between 18 GHz and 37 GHz, the average slope is slightly smaller.

VII. VOLUME SCATTERING BY SNOW

So far we have examined the permittivity of dry snow and both the permittivity and dielectric loss factor of wet snow. Now we shall present results related to the extinction loss in dry snow.

As was mentioned earlier, scattering losses in dry snow are a significant component of the total extinction loss, particularly at the higher microwave frequencies. Also, the shapes and sizes of the ice crystals are important factors. Figure 16 shows the results of loss measurements for four snow types at 37 GHz. Three of the samples had undergone one or more melt-freeze cycles, whereas the fourth was made of newly fallen snow. The density of the newly fallen snow sample was slightly lower than the densities of the other samples, but the difference is not sufficiently large to explain the large difference in extinction loss. However, the average diameters of the ice crystals (as estimated from photographs obtained using a fiber-optic microscope) were between 1.4 mm and 1.5 mm for the metamorphosed snow samples, compared to 1.0 mm for the newly fallen snow sample. According to Mie calculations, increasing the particle diameter from 1.0 mm to 1.5 mm leads to more than a two-fold increase in the extinction coefficient κ_e.

VII. CONCLUSIONS

The following conclusions were drawn from this study of the dielectric behavior of snow in the 3- to 37-GHz range:

(1) The dielectric constant of dry snow increases almost linearly with increasing snow density.

(2) The dispersion behavior of water determines the spectral behavior of wet snow. The relaxation frequency of wet snow is approximately 9.0 GHz, which is similar to that of liquid water.

(3) Above 14 GHz, volume scattering is the dominant loss mechanism in dry snow for a snow-particle size of 1 mm or larger. The scattering loss decreases rapidly with increasing liquid water content, becoming negligible for m_v values above 1 percent.

(4) Of the empirical models developed, the modified Debye-like model best describes the dielectric behavior of snow as a function of its physical parameters and frequency.

(5) If nonsymmetry is assumed for the depolarization factors of the water inclusions, both the two-phase and three-phase Polder-Van Santen models describe the dielectric behavior of snow equally well.

(6) As water appears in the snow, the water inclusions become needle-like in shape. A transition in shape occurs around m_v = 3%, at which point the inclusions become disc-like. These results were obtained by optimizing the shape of the water inclusions to fit the two-phase and three-phase Polder-Van Santen models to the measured values of ε''_{ws}.

REFERENCES

[1] Gray, D. M., and D. H. Male, Eds., Handbook of Snow: Principles, Processes, Management and Use. New York: Pergamon Press, 1981.

[2] Colbeck, S. C., "The geometry and permittivity of snow at high frequencies," J. Appl. Physics, vol. 53, pp. 4495-4500, 1982.

[3] Ulaby, F. T., R. K. Moore, and A. K. Fung, Microwave Remote Sensing: Active and Passive. Vols. I and III. Addison-Wesley/Benjamin-Cummings, Menlo Park, CA, 1982-1985.

[4] Stiles, W. H., and F. T. Ulaby, "The active and passive microwave response to snow parameters, Part I: Wetness," J. Geophys. Res., vol. 83, pp. 1037-1044, 1980.

[5] Ulaby, F. T., and W. H. Stiles, "The active and passive microwave response to snow parameters, Part II: Water equivalent of dry snow," J. Geophys. Res., vol. 83, pp. 1045-1049, 1980.

[6] Hofer, R., and C. Mätzler, "Investigations on snow parameters by radiometry in the 3- to 60-mm wavelength region," J. Geophys. Res., vol. 85, pp. 453-460, 1980.

[7] Tiuri, M., "Theoretical and experimental studies of microwave emission signatures of snow," IEEE Trans. Geosci. Remote Sensing, vol. GE-20, pp. 51-57, 1982.

[8] Mätzler, C., E. Schanda, and W. Good, "Towards the definition of optimum sensor specifications for microwave remote sensing of snow," IEEE Trans. Geosci. Remote Sensing, vol. GE-20, pp. 57-66, 1982.

[9] Künzi, K., S. Patil, and H. Rott, "Snow-cover parameters retrieved from Nimbus-7 scanning multichannel microwave radiometer (SMMR)

data," IEEE Trans. Geosci. Remote Sensing, vol. GE-20, pp. 452-467, 1982.

[10] Hallikainen, M., "Remote sensing of the water equivalent of snow cover by passive microwave satellite observations," 1983 IEEE Int. Geosci. Remote Sensing Symp. (IGARSS'83) Digest, San Francisco, CA, 31 August-2 September, 1983.

[11] Cumming, W., "The dielectric properties of ice and snow at 3.2 centimeters," J. Appl. Phys., vol. 23, pp. 768-773, 1952.

[12] Sweeney, B. D., and S. C. Colbeck, "Measurements of the dielectric properties of wet snow using a microwave technique," Research Report 325, U. S. Army Cold Regions Research and Engineering Laboratory, Hanover, NH, 1974.

[13] Tobarias, J., D. Saguet, and J. Chilo, "Determination of the water content of snow from the study of electromagnetic wave propagation in the snow cover," J. Glaciol., vol. 20, pp. 585-592, 1980.

[14] Linlor, W. I., "Permittivity and attenuation of wet snow between 4 and 12 GHz," J. Appl. Phys., vol. 51, pp. 2811-2816, 1980.

[15] Nyfors, E., "On the dielectric properties of dry snow in the 800 MHz to 13 GHz region," Report 5135, Helsinki University of Technology, Radio Laboratory, Otaniemi, Finland, 1983.

[16] Glen, J. W., and P. G. Paren, "The electrical properties of snow and ice," J. Glaciol., vol. 15, pp. 15-38, 1975.

[17] Colbeck, S. C., "Liquid distribution and the dielectric constant of wet snow," NASA Workshop on Microwave Remote Sensing of Snowpack Properties, NASA CP2153, Ft. Collins, CO, May 20-22, 1980.

[18] Ambach, W., and A. Denoth, "The dielectric behavior of snow: A study versus liquid water content," NASA Workshop on Microwave Remote Sensing of Snowpack Properties, NASA CP-2153, Ft. Collins, CO, May 20-22, 1980.

[19] Tiuri, M., and H. Schultz, "Theoretical and experimental studies of microwave radiation from a natural snow field," NASA Workshop on Microwave Remote Sensing of Snowpack Properties, NASA CP-2153, Ft. Collins, CO, May 20-22, 1980.

[20] Hallikainen, M., F. T. Ulaby, M. C. Dobson, M. El-Rayes and L. Wu, "Micorwave dielectric behavior of wet soil - Part I: Empirical models and experimental observations," IEEE Trans. Geos. and Rem. Sensing, vol. GE-23, pp. 25-34, 1985.

[21] Hallikainen, M., F. T. Ulaby, M. Abdelrazik, and D. R. Brunfeldt, "A 37-GHz free-space system for dielectric measurements," Remote Sensing Laboratory Tech. Rep. 333-1, University of Kansas Center for Research, Inc., Lawrence, KS, 1984.

[22] Von Hippel, A., Ed., Dielectric materials and applications. MIT Press: Cambridge, MA, 1954.

[23] Ambach, W., and A. Denoth, "Studies on the dielectric properties of snow," Zeitschrift für Gletscherkunde und Glazialgeologie, Bd VIII, Heft 1-2, pp. 113-123, 1972.

[24] Evans, S., "Dielectric properties of ice and snow--A review," J. Glaciol., vol. 5, pp. 773-792, 1965.

[25] Hallikainen, M., "Measured permittivities of snow and low-salinity sea ice for UHF radiometer applications," Swedish National Convention on Radio Science, Stockholm, Sweden, March 29-31, 1978.

[26] Tiuri, M., A. Sihvola, and E. Nyfors, "The complex dielectric constant of snow at UHF frequencies," EARSeL WG on Microwave Remote Sensing of Snow, Snow Wetness Workshop, Berne, Switzerland, 1983.

[27] Polder, D., and J. H. Van Santen, "The effective permeability of mixtures of solids," Physica, vol. 12, pp. 257-271, 1946.

[28] Stiles, W. H., and F. T. Ulaby, "Dielectric properties of snow," Remote Sensing Laboratory Tech. Rep. 527-1, University of Kansas Center for Research, Inc., Lawrence, KS, 1981.

[29] Tinga, W. R., W. A. G. Voss, and D. F. Blossey, "Generalized approach to multiphase dielectric mixture theory," J. Appl. Phys., vol. 44, pp. 3897-3902, 1973.

[30] de Loor, G. P., "Dielectric properties of heterogeneous mixtures with a polar constituent," Appl. Sci. Res., Section B, vol. II, pp. 310-319, 1964.

[31] Birchak, J. R., C. G. Gardner, J. E. Hipp, and J. M. Victor, "High dielectric constant microwave probes for sensing soil moisture," Proc. IEEE, vol. 62, pp. 93-98, 1974.

[32] H. J. Eom, K. K. Lee, and A. K. Fung, "Microwave emission from an irregular snow layer," Remote Sensing of Environment, vol. 13, pp. 423-437, 1983.

FIGURE CAPTIONS

Figure 1. Calculated extinction coefficient κ_e, scattering coefficient κ_s, and absorption coefficient κ_a for dry snow as a function of frequency.

Figure 2. Calculated (a) scattering albedo and (b) penetration depth as a function of liquid-water content at 4 GHz, 10 GHz, and 37 GHz.

Figure 3. Block diagram of the (a) 3- to 18-GHz and (b) 37-GHz free-space transmission systems.

Figure 4. Calculated worst-case error bounds for (a) measured snow permittivity and (b) measured loss factor as a function of frequency, with volumetric water content and sample thickness as parameters.

Figure 5. Comparison of the 1982 and 1983 measurements for (a) the dielectric constant and (b) the loss factor of snow at 18 GHz.

Figure 6. Measured permittivity of dry snow over the 3-37 GHz region as a function of density ρ_{ds} for $\rho_{ds} < 0.5$.

Figure 7. Variation of ε'_{ds} with ρ_{ds}.

Figure 8. Comparison of Eq. (13) with Cumming's experimental data [11] for the loss factor of dry snow relative to that of ice.

Figure 9. Depolarization factors A_{w1}, A_{w2}, and A_{w3} for water inclusions in snow, optimized by fitting the two-phase Polder-Van Santen model to the measured values of ε''_{ws}.

Figure 10. Comparison of model predictions with measured values of $\Delta\varepsilon'_{ws}$ and ε''_{ws} at 6 GHz.

Figure 11. Comparison of model predictions with measured values of $\Delta\varepsilon'_{ws}$ and ε''_{ws} at 37 GHz.

Figure 12. Comparison of the two-phase Polder-Van Santen model predictions with experimental data for (a) ε'_{ws} and (b) ε''_{ws}.

Figure 13. Dielectric constant of snow according to the modified Debye-like model plotted as a function of frequency, with liquid-water content as a parameter.

Figure 14. Loss factor of snow, according to the modified Debye-like model, plotted as a function of frequency with liquid-water content as a parameter.

Figure 15. Attenuation coefficient of snow according to the modified Debye-like model, plotted as a function of frequency with liquid-water content as a parameter.

Figure 16. Measured total loss for four dry snow types at 37 GHz.

Table 1. Summary of Microwave Dielectric Measurements of Snow.

Frequency (GHz)	Snow Density (g/cm^3)	Liquid Water Content (%)	Crystal Size Diameter (mm)	Temperature T(°C)	Reference and Year
9.375	0.34 - 0.916	0	not reported	-18 to 0	Cumming [11] 1952
9.375	0.38, 0.76	0-1.2	not reported	0	Cumming [11] 1952
6	0.6	0-24.4	not reported	0	Sweeny and Colbeck [12] 1974
9.4	0.5	0-9.0	not reported	0	Tabarias et al. [13] 1978
4-12	0.30 - 0.60	0-12.0	0.1 - 1.0	0	Linlor [14] 1980
0.8-13	0.07 - 0.53	0	not reported	-30 to -5	Nyfors [15] 1983
3-18 & 37	0.09 - 0.42	0-12.3	0.5 - 1.5	-5 to 0	present study

Table 2. Effect of the Shape of Water Inclusions on the Capability of the Two-Phase Polder and Van Santen Model to Describe the Dielectric Behavior of Snow in the 3- to 37-GHz Range (955 Data Points).

	Model							
	Shape of Water Inclusions Symmetrical, A_{wi} Optimized Using ε_{ws}' Data		Shape of Water Inclusions Symmetrical, A_{wi} Optimized Using ε_{ws}'' Data		Shape of Water Inclusions Nonsymmetrical, Independent of Water Content of Snow, A_{wi} Optimized Using ε_{ws}'' Data		Shape of Water Inclusions Nonsymmetrical, Depends on Water Content of Snow, A_{wi} Optimized Using ε_{ws}'' Data	
Parameter	ε_{ws}'	ε_{ws}''	ε_{ws}'	ε_{ws}''	ε_{ws}'	ε_{ws}''	ε_{ws}'	ε_{ws}''
A_{w1}	0.155		0.074		0.067			
A_{w2}	0.155		0.074		0.251		See Figure 9	
A_{w3}	0.690		0.852		0.682		for values of A_{wi}	
Residual Sum of Squares	7.965	25.079	64.246	4.702	8.592	2.997	4.399	2.611
Linear Correlation Coefficient	0.978	0.961	0.981	0.962	0.984	0.975	0.988	0.978
α', α''	1.001	1.791	0.700	0.957	1.116	0.989	1.025	0.996
β', β''	-0.012	0.031	0.398	0.020	-0.160	0.005	-0.040	-0.003

$$\varepsilon_{ws}'(\text{obs}) = \alpha'\varepsilon_{ws}'(\text{pred}) + \beta'$$

$$\varepsilon_{ws}''(\text{obs}) = \alpha''\varepsilon_{ws}''(\text{pred}) + \beta''$$

Table 3. rms Errors for ε'_{ws} and ε''_{ws} Computed According to (8) Using 955 Data Points Covering the 3-37 GHz Range.

Model	e'_{rms}	e''_{rms}
Two-Phase Polder-Van Santen, Eq. (14)	0.067	0.052
Three-Phase Polder-Van Santen, Eq. (15)	0.065	0.053
Debye-Like, Eqs. (16) - (18)	0.070	0.091
Modified Debye-Like, Eqs. (16) - (19)	0.068	0.060

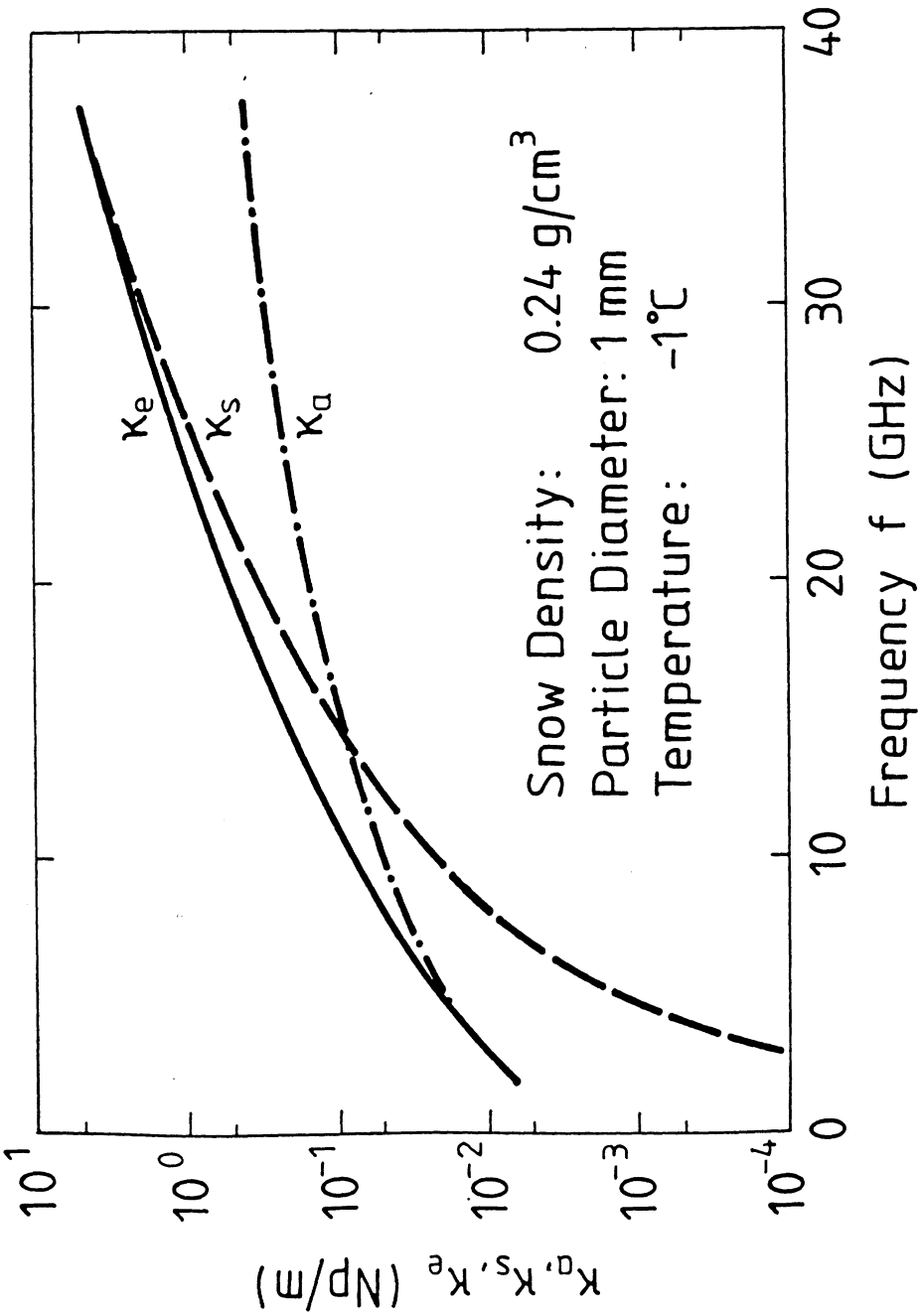

Hallikainen, Ulaby, Abdelrazik
Figure 1

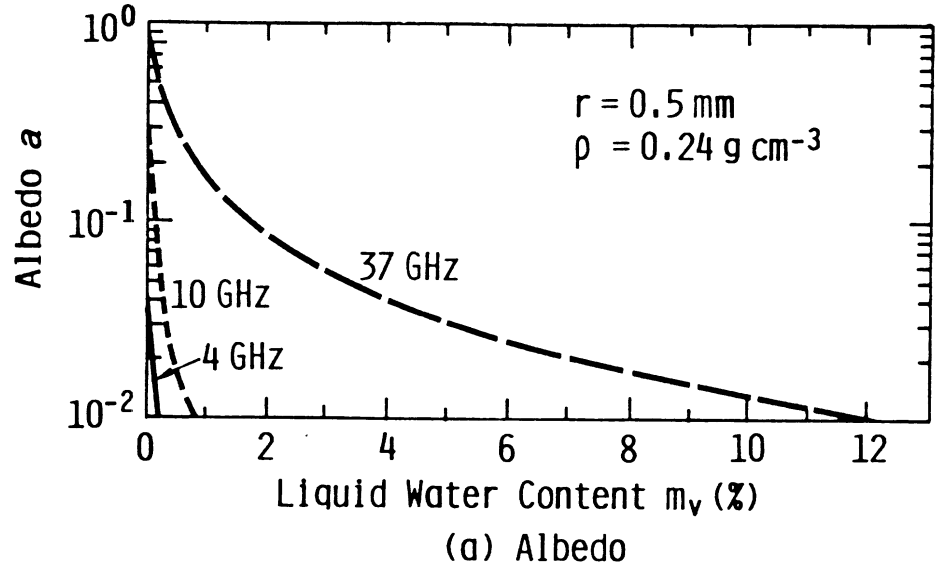

(a) Albedo

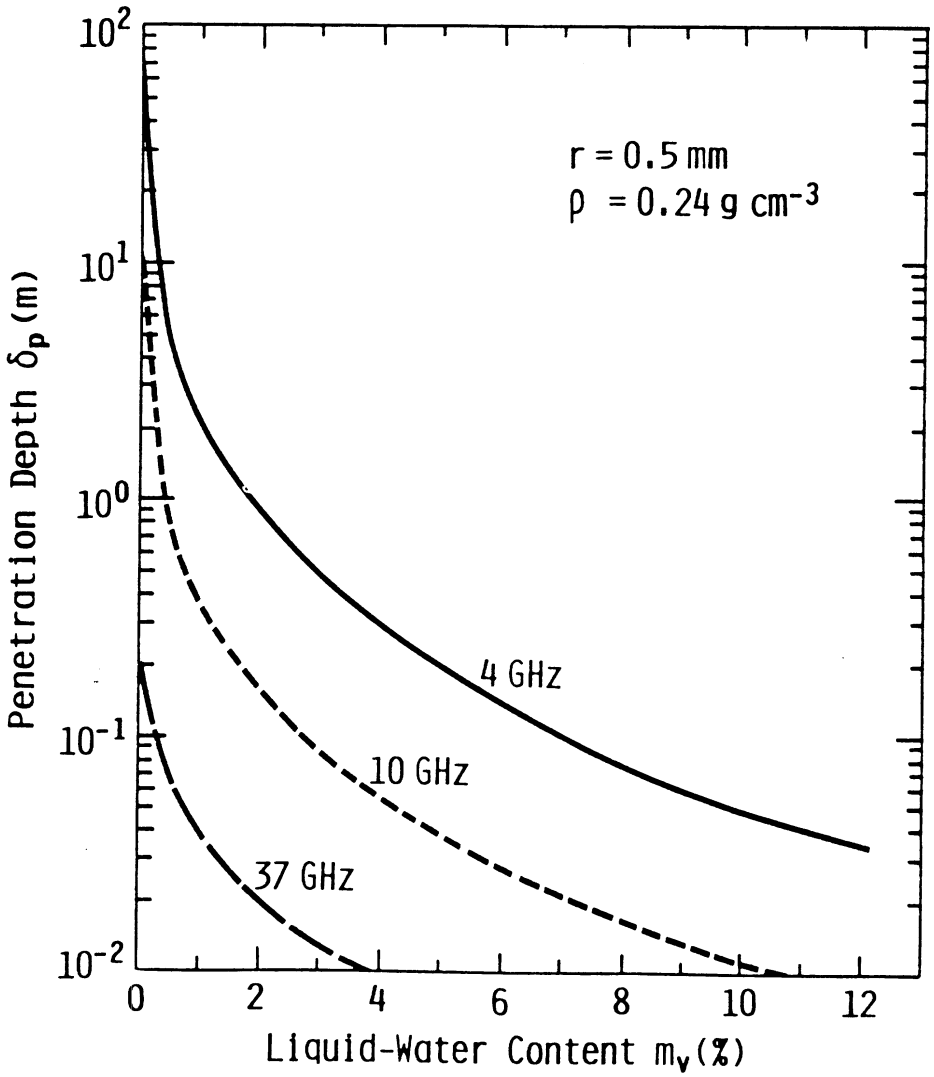

(b) Penetration Depth

Hallikainen, Ulaby, Abdelrazi
Figure 2

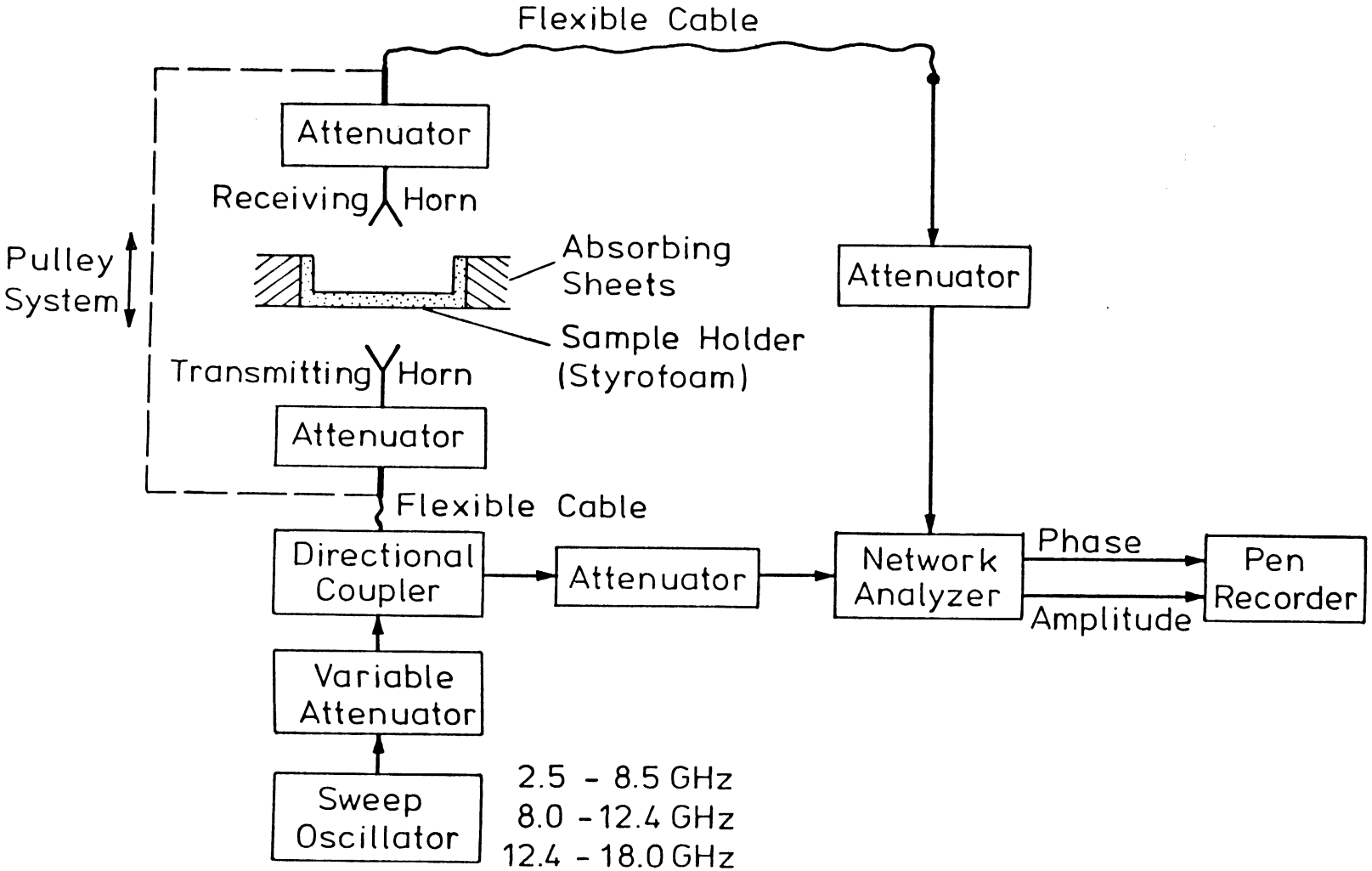

Hallikainen, Ulaby, Abdelrazi
Figure 3a

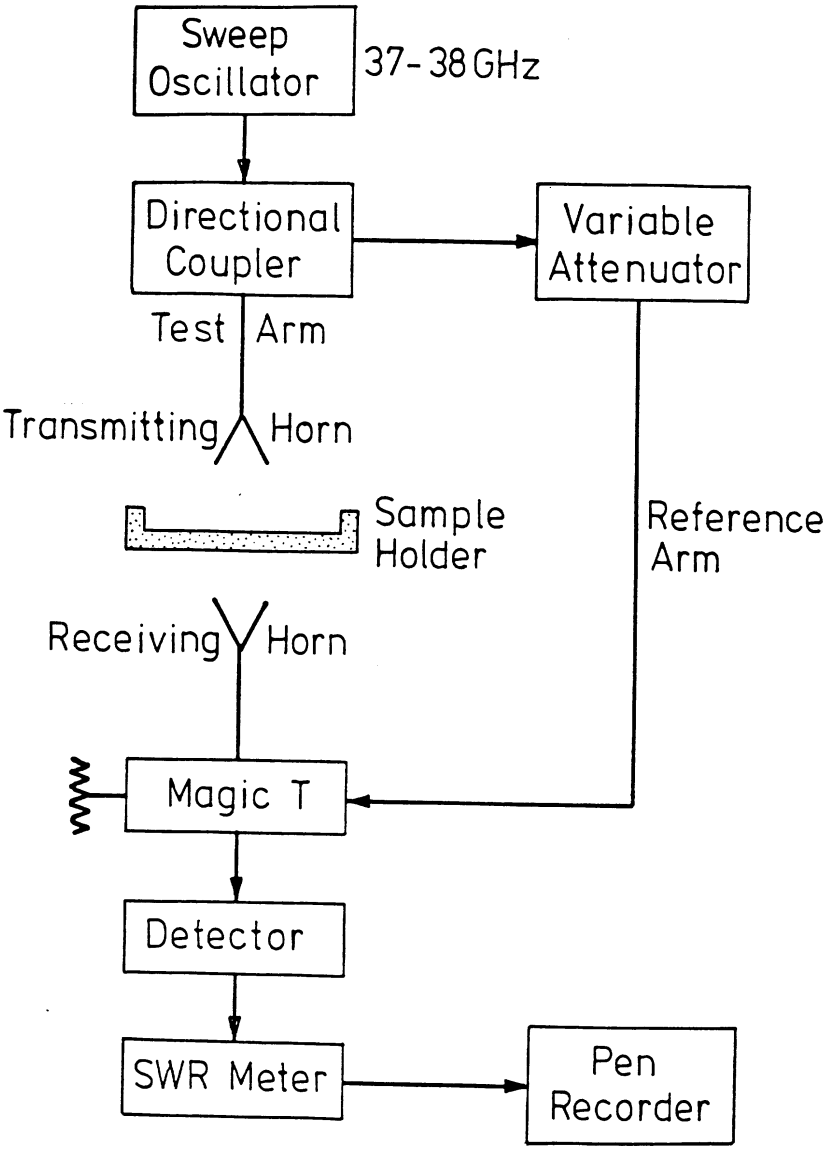

Hallikainen, Ulaby, Abdelrazil
Figure 3b.

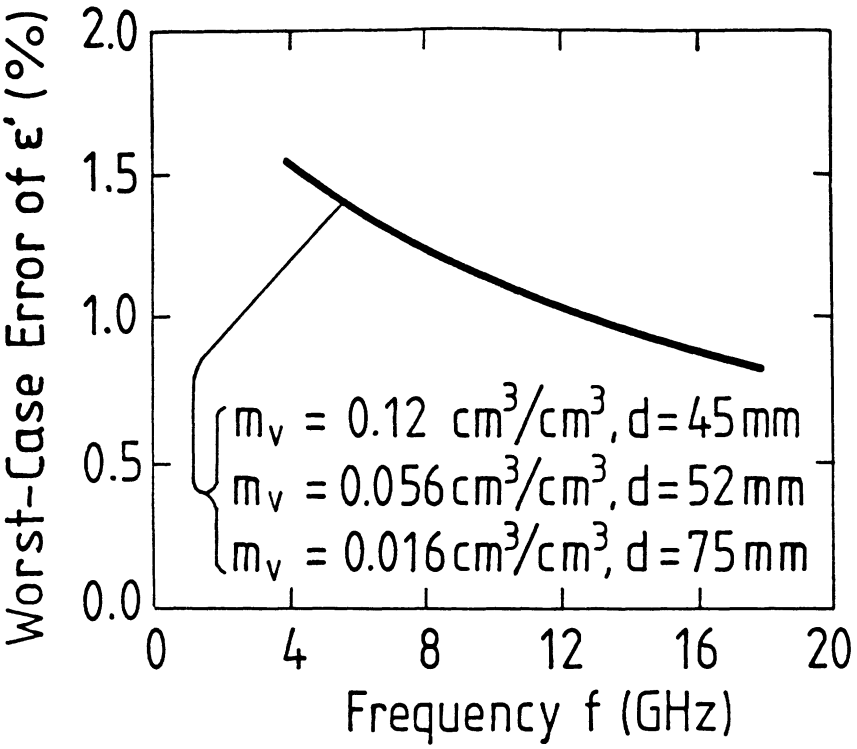

(a)

Hallikainen, Ulaby, Abdelraz
Figure 4(a)

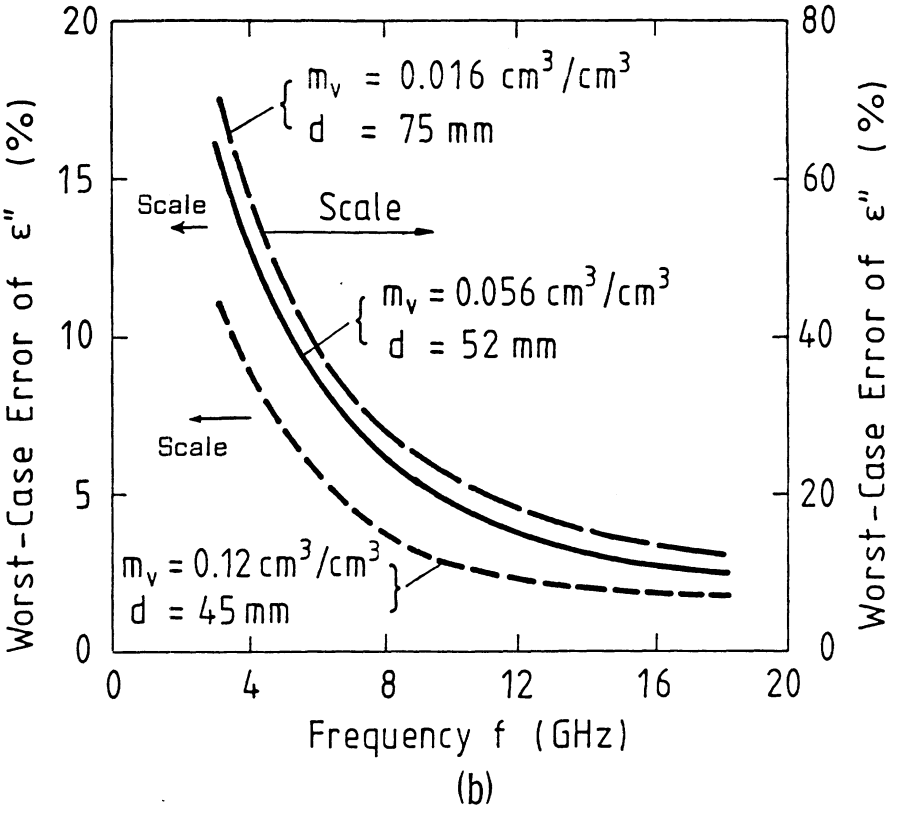

(b)

Hallikainen, Ulaby, Abdelrazik
Figure 4(b)

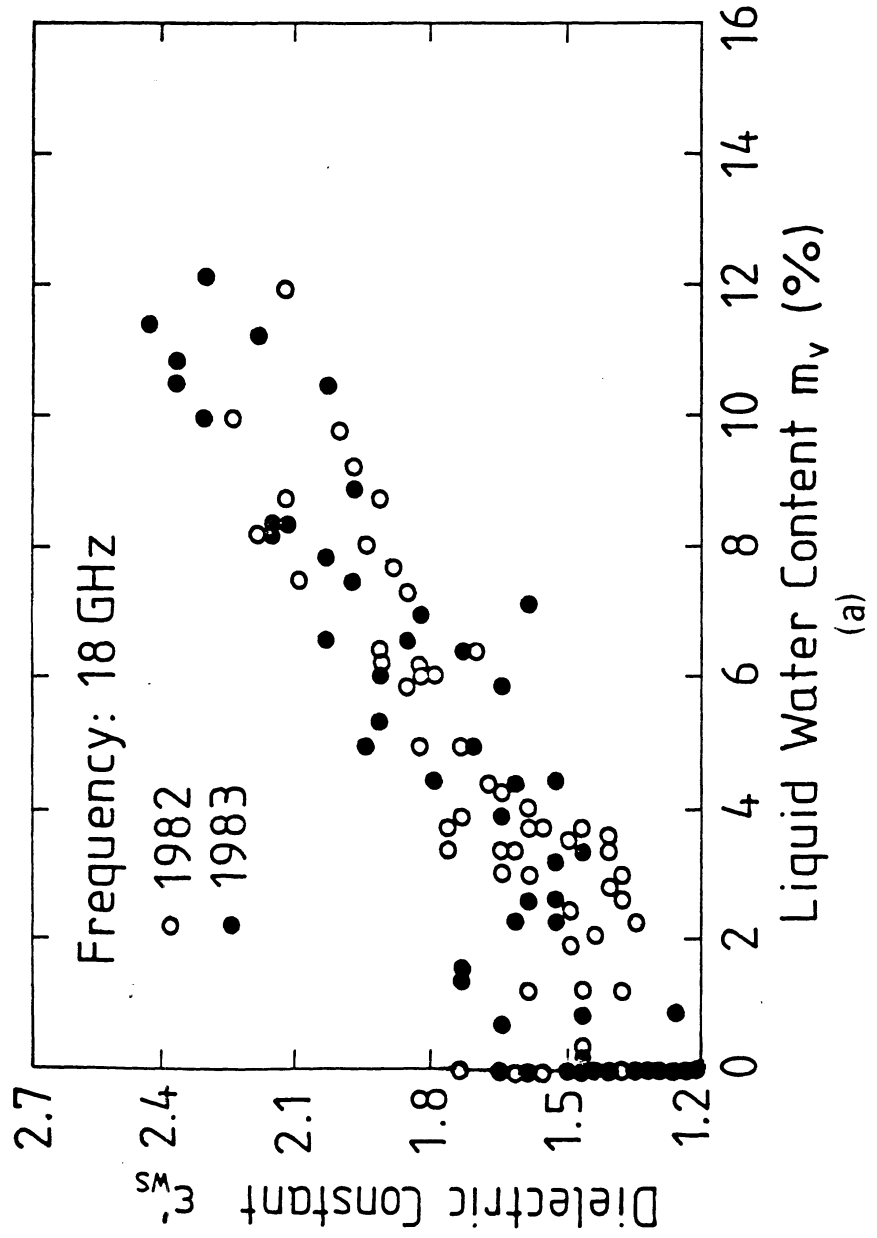

Hallikainen, Ulaby, Abdelrazik
Figure 5(a)

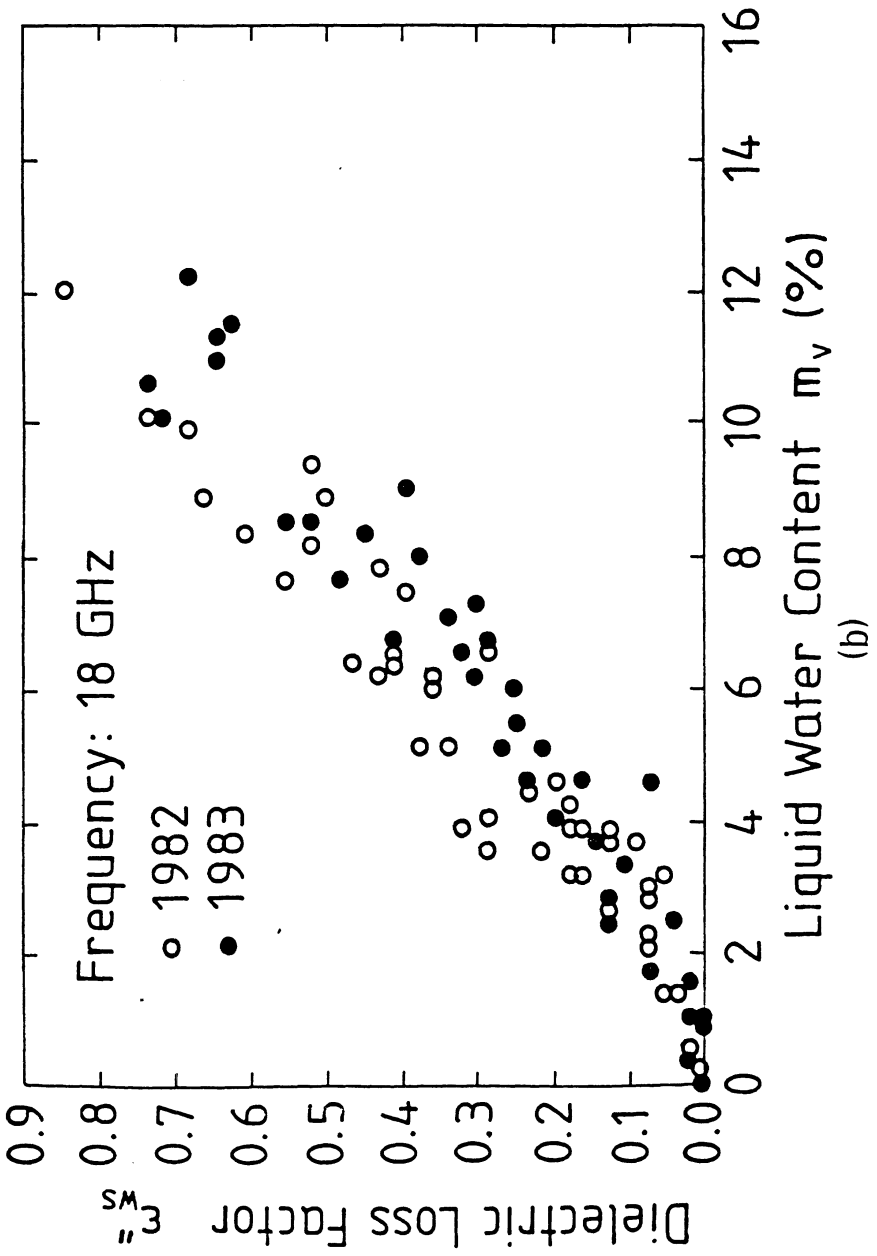

Hallikainen, Ulaby, Abdelrazik
Figure 5(b)

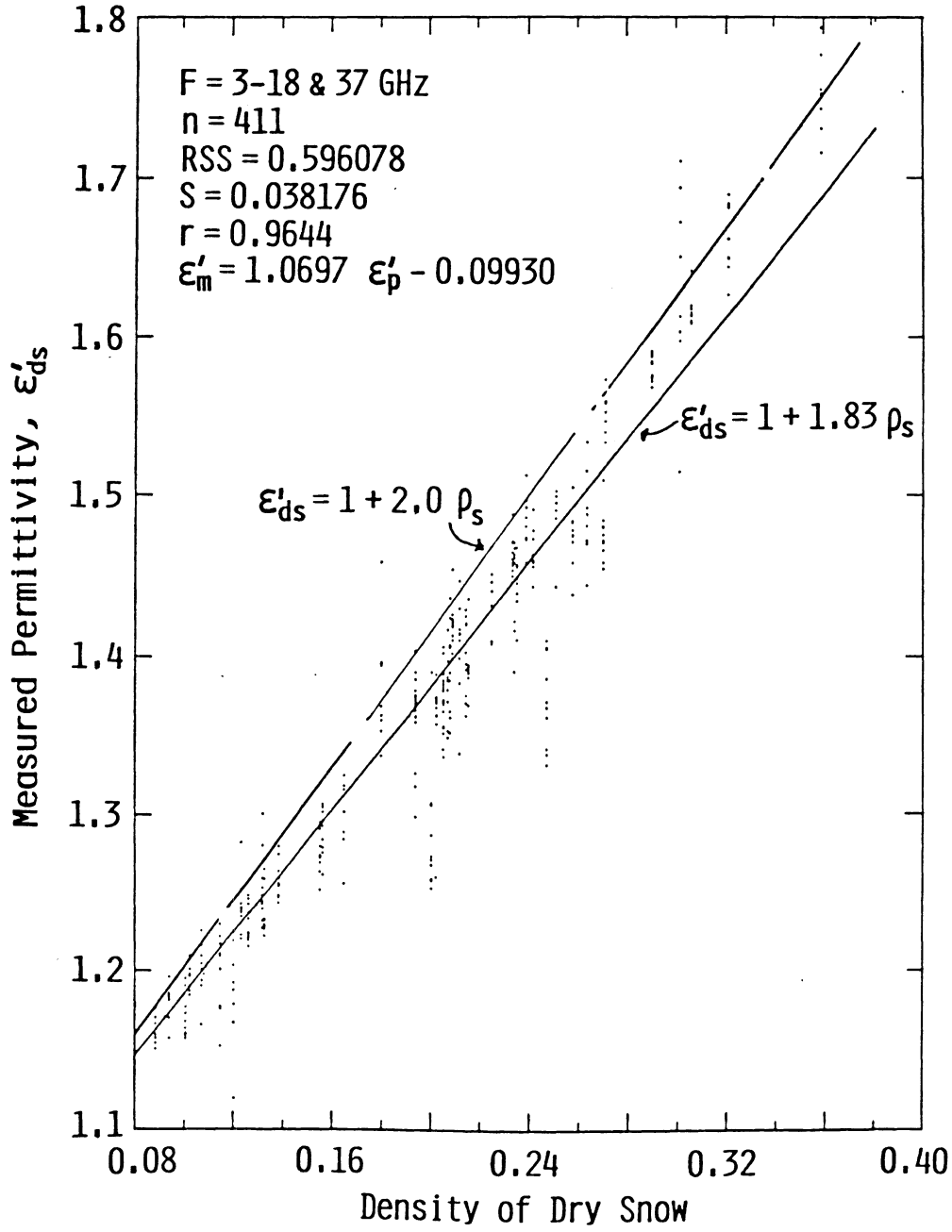

Hallikainen, Ulaby, Abdelrazik
Figure 6

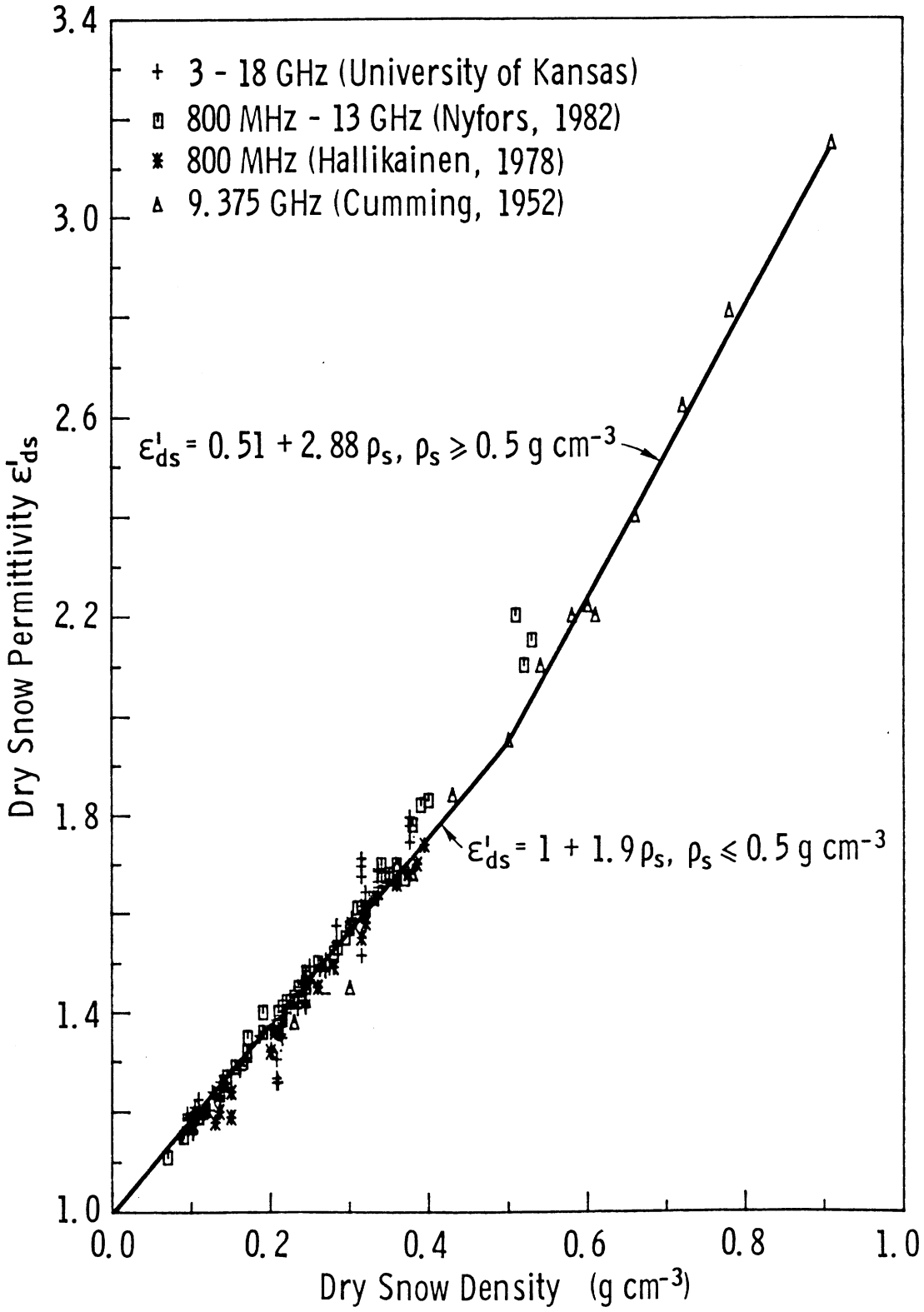

Hallikainen, Ulaby, Abdelrazi
Figure 7

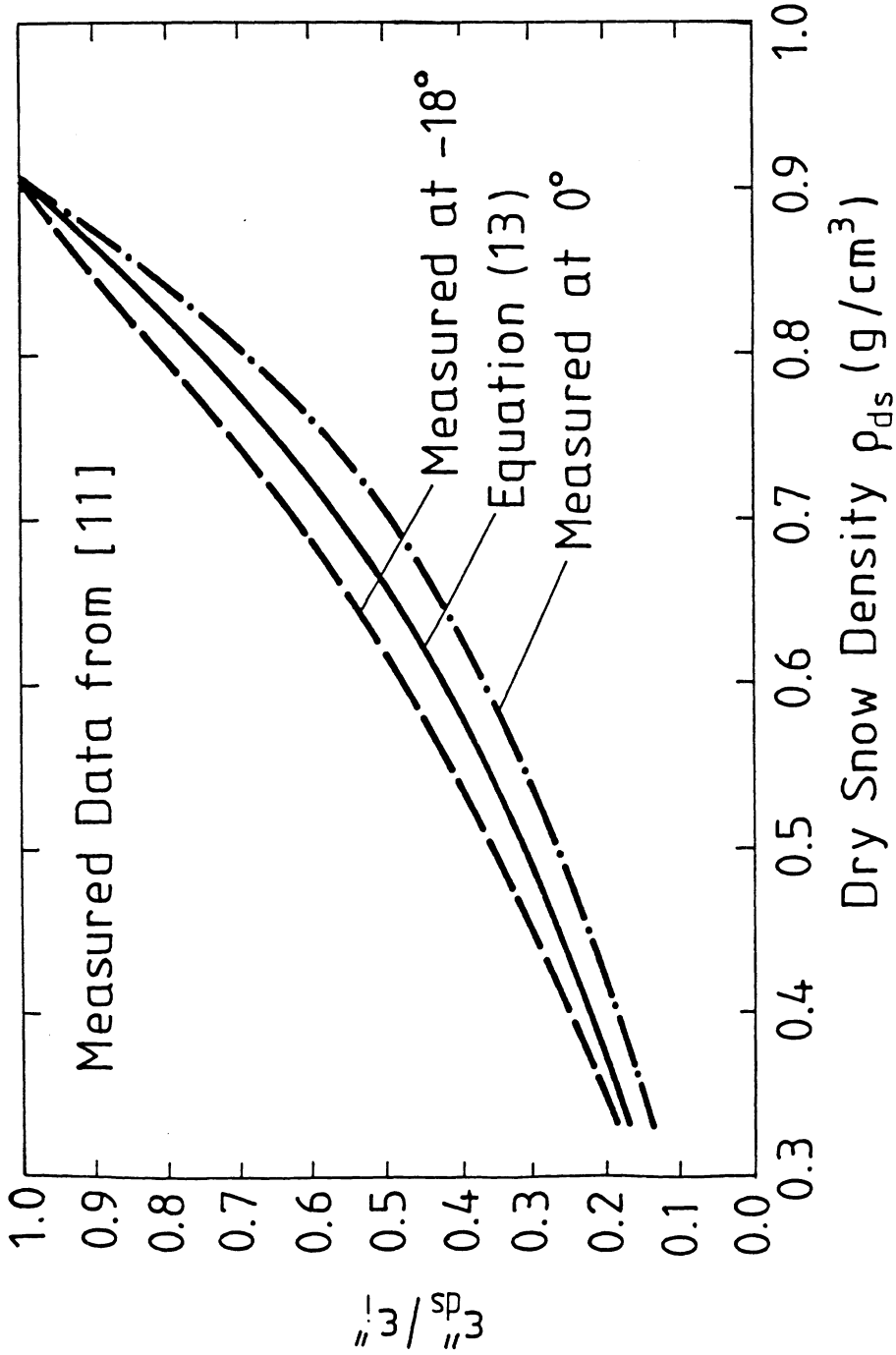

Hallikainen, Ulaby, Abdelrazik
Figure 8

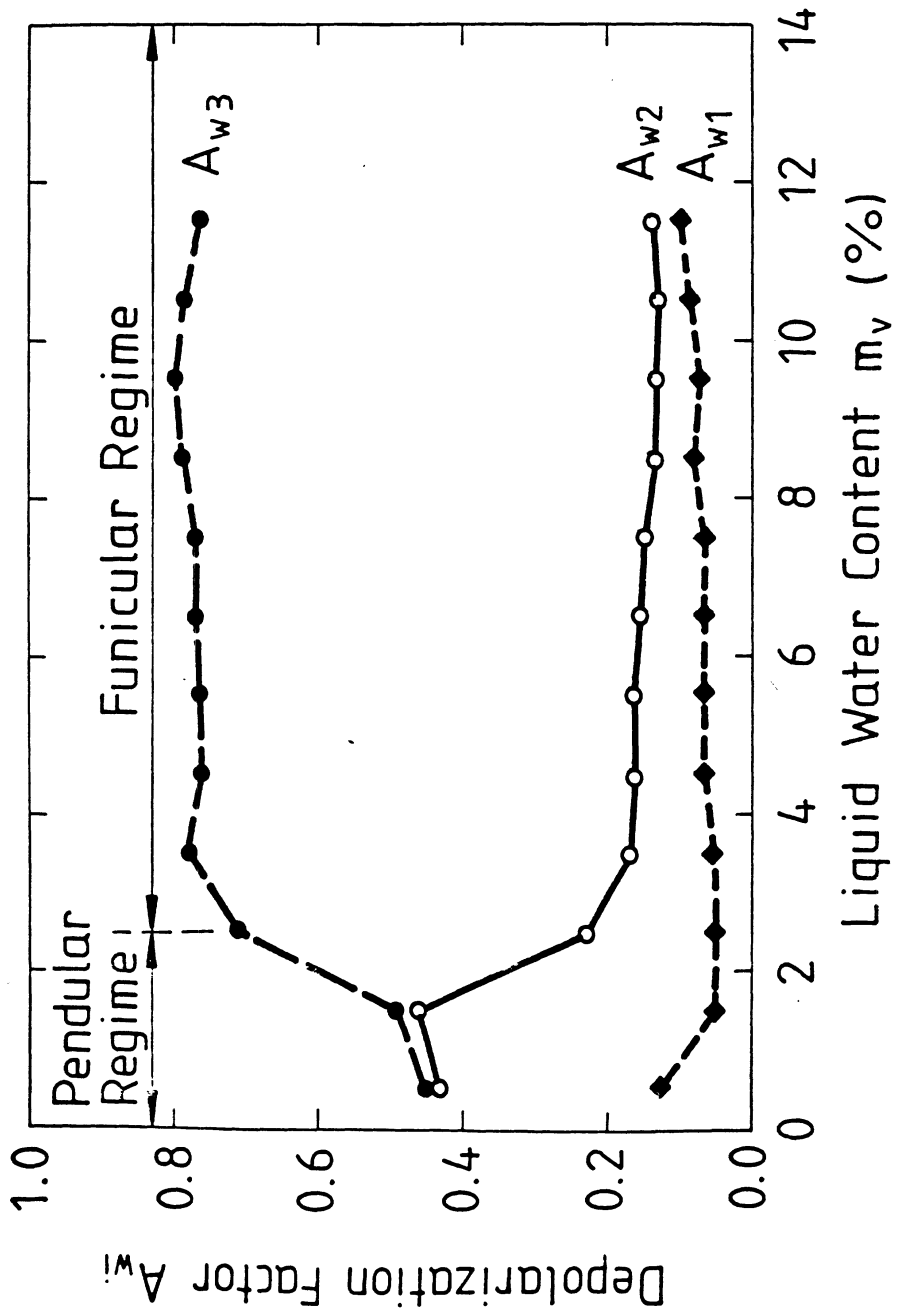

Hallikainen, Ulaby, Abdelraz
Figure 9

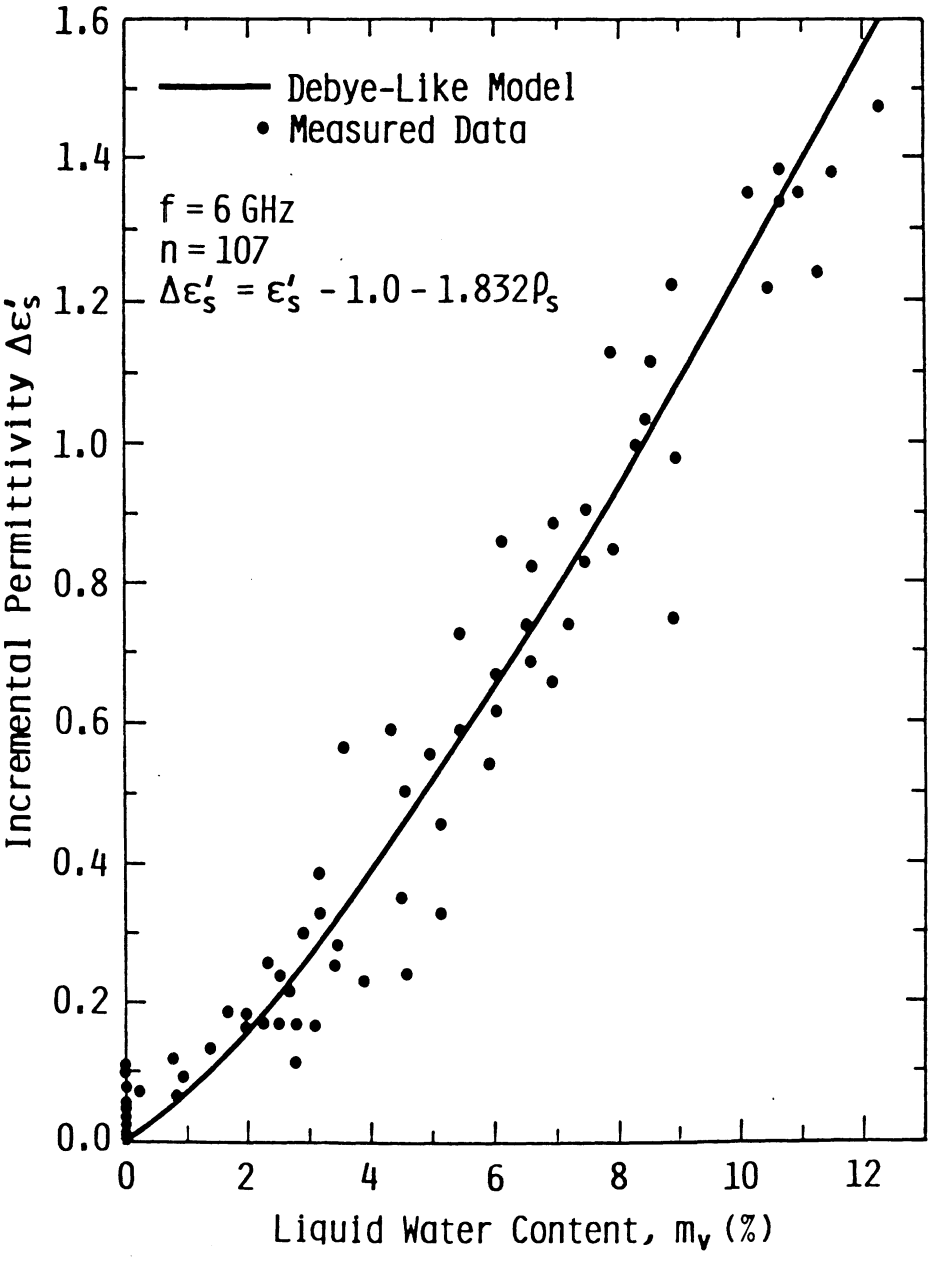

(a) Incremental Permittivity

Hallikainen, Ulaby, Abdelrazik
Figure 10(a)

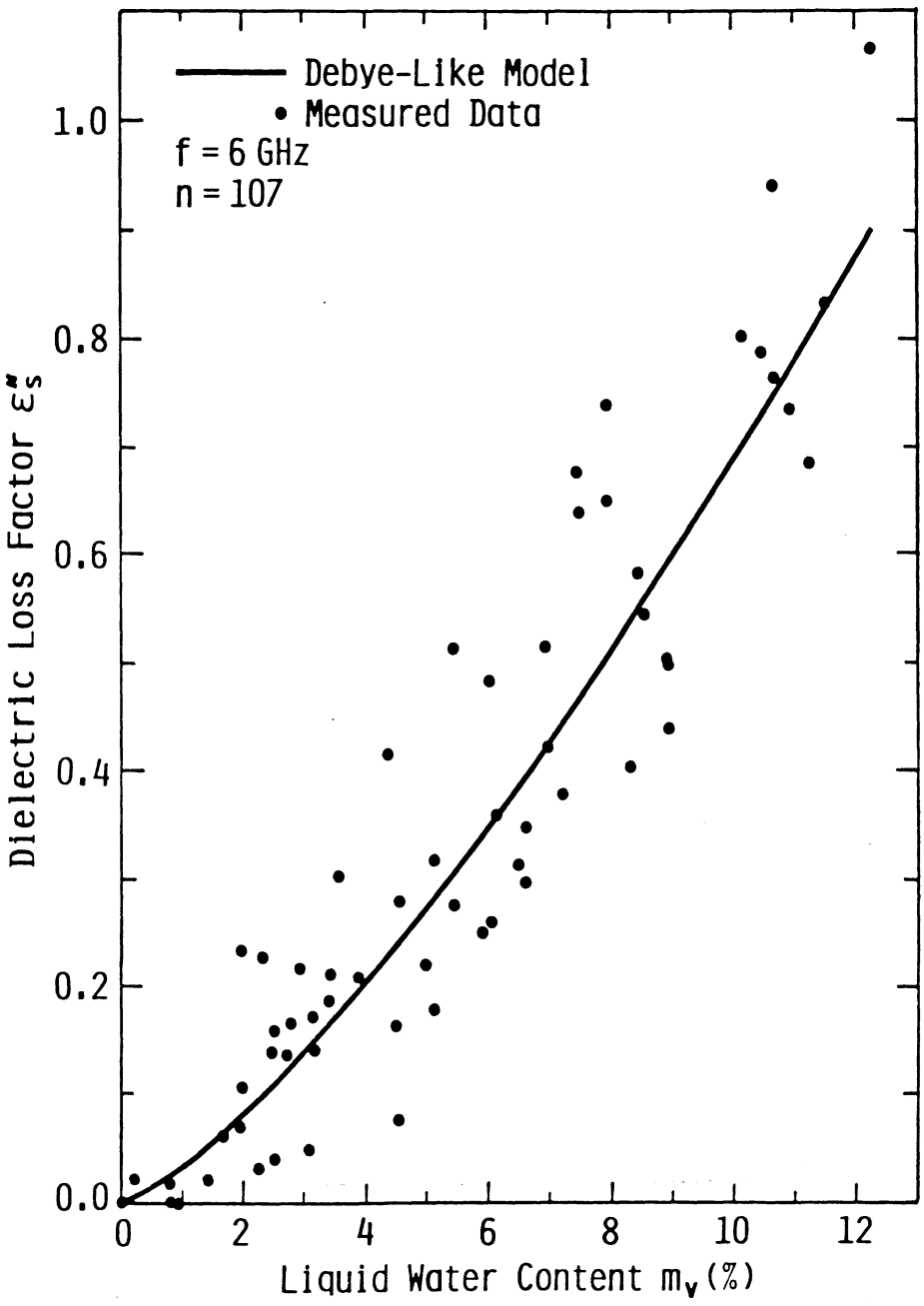

(b) Loss Factor

Hallikainen, Ulaby, Abdelrazik
Figure 10(b)

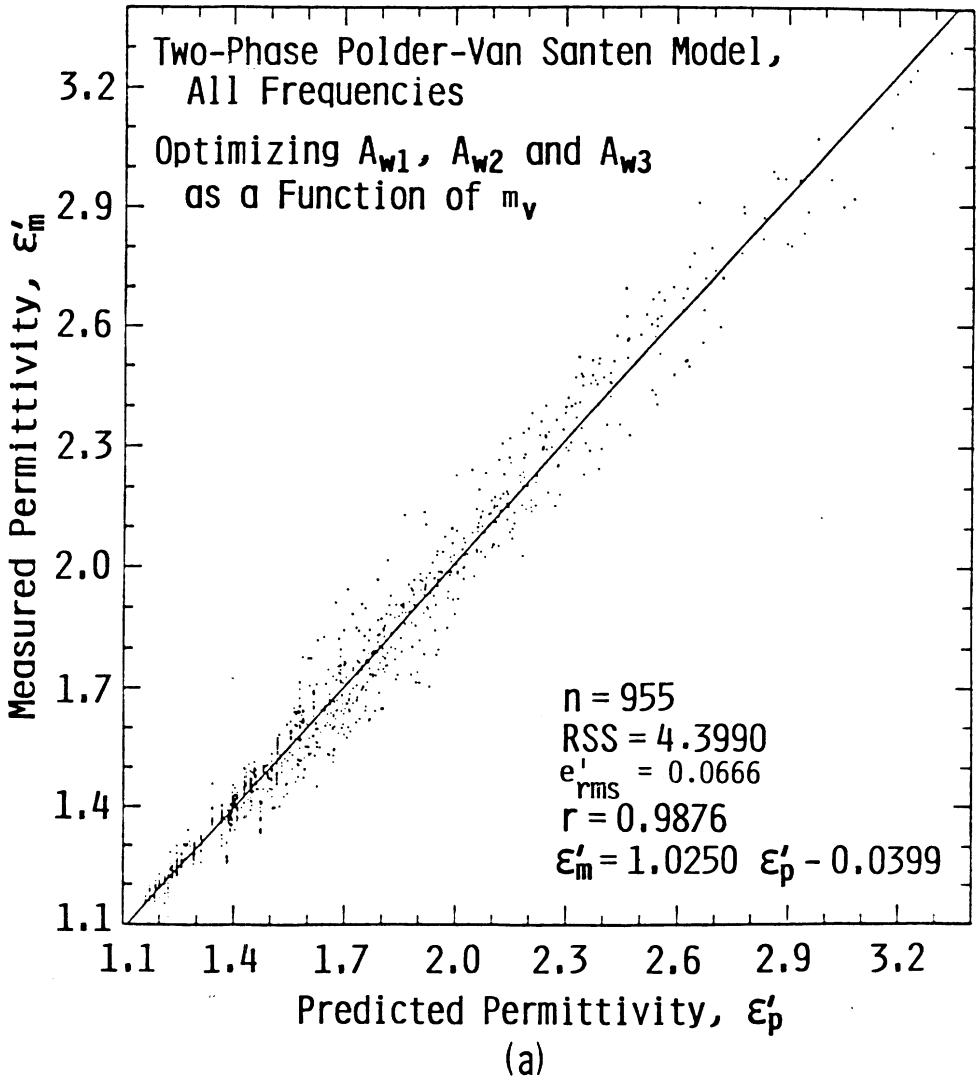

(a)

Hallikainen, Ulaby, Abdelrazik
Figure 12(a)

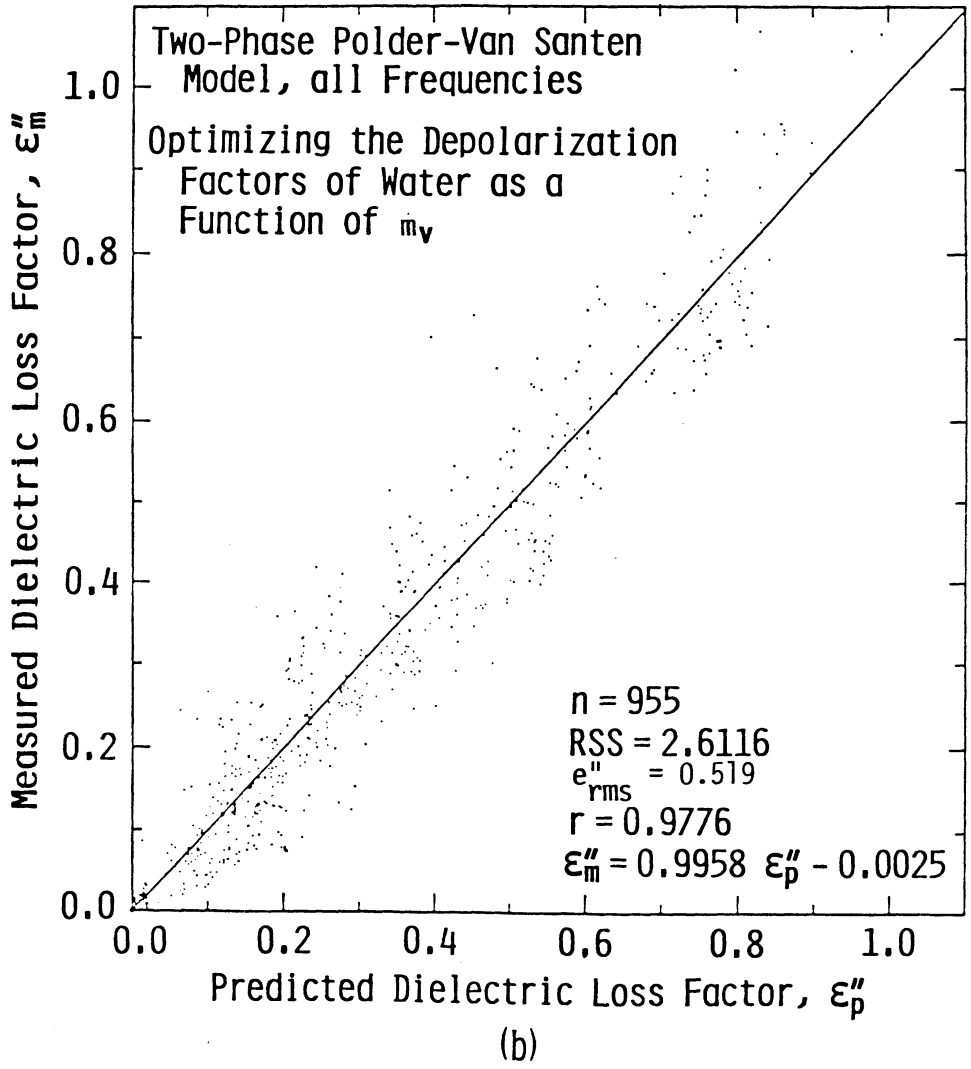

(b)

Hallikainen, Ulaby, Abdelrazik
Figure 12(b)

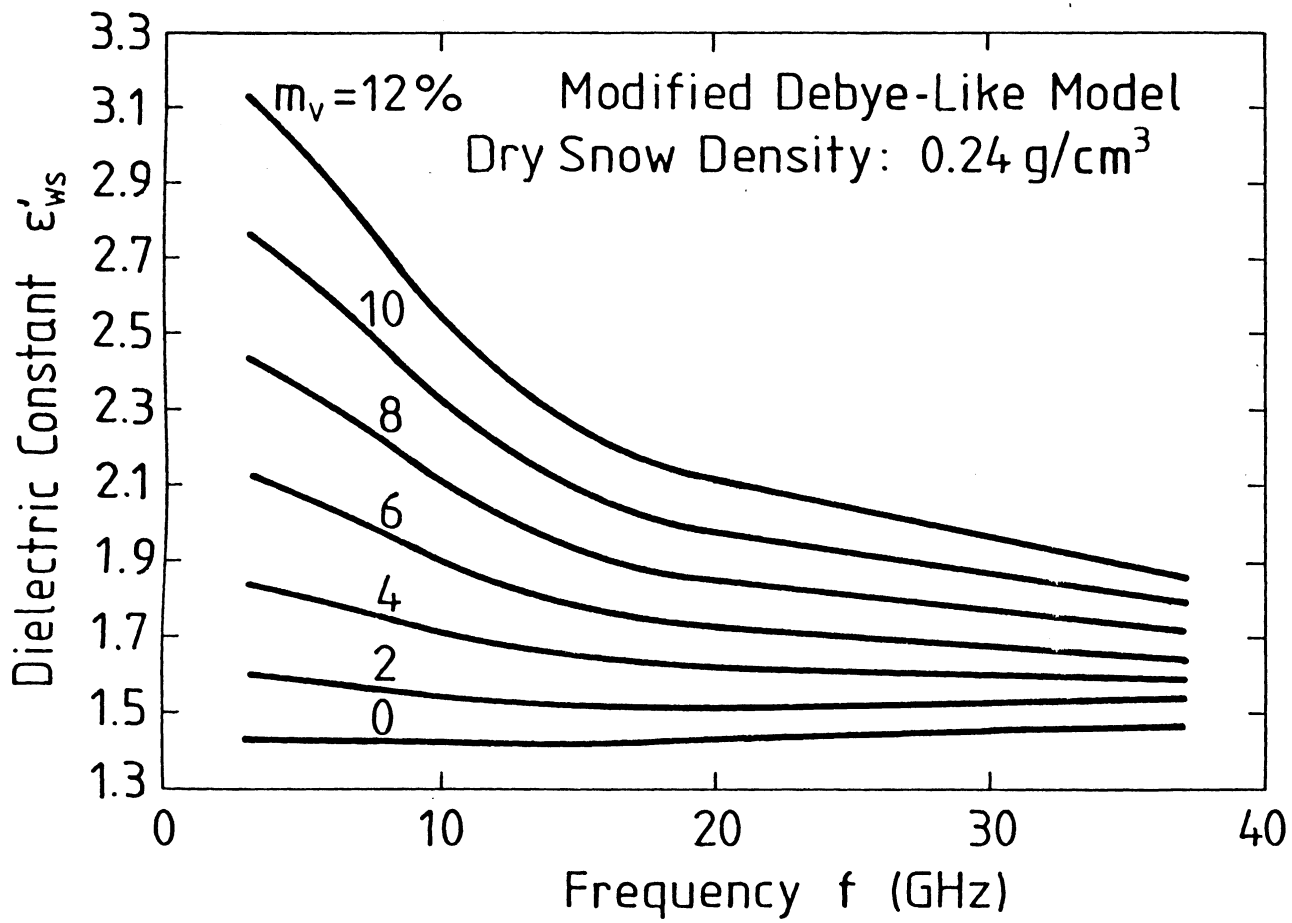

Hallikainen, Ulaby, Abdelrazik
Figure 13

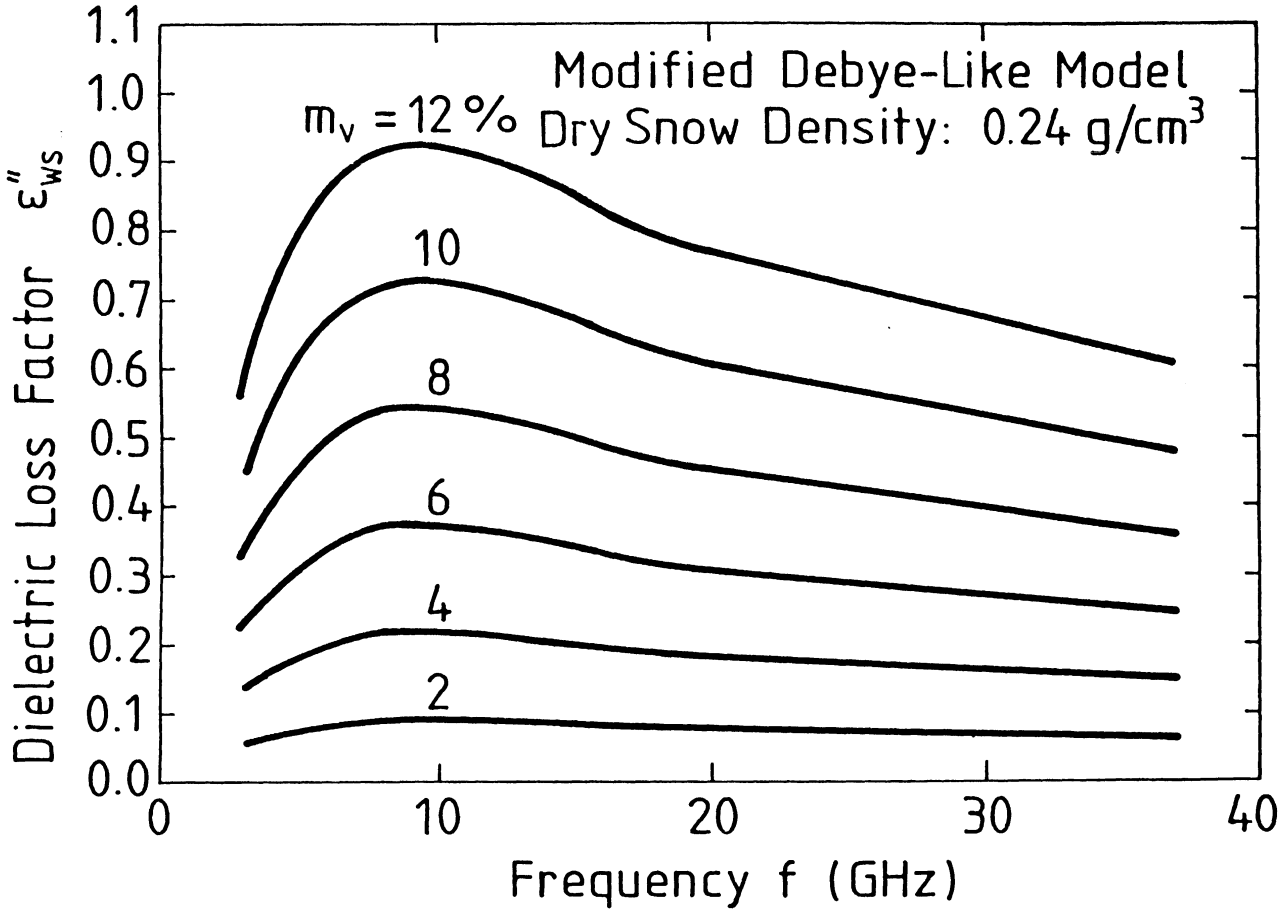

Hallikainen, Ulaby, Abdelrazik
Figure 14

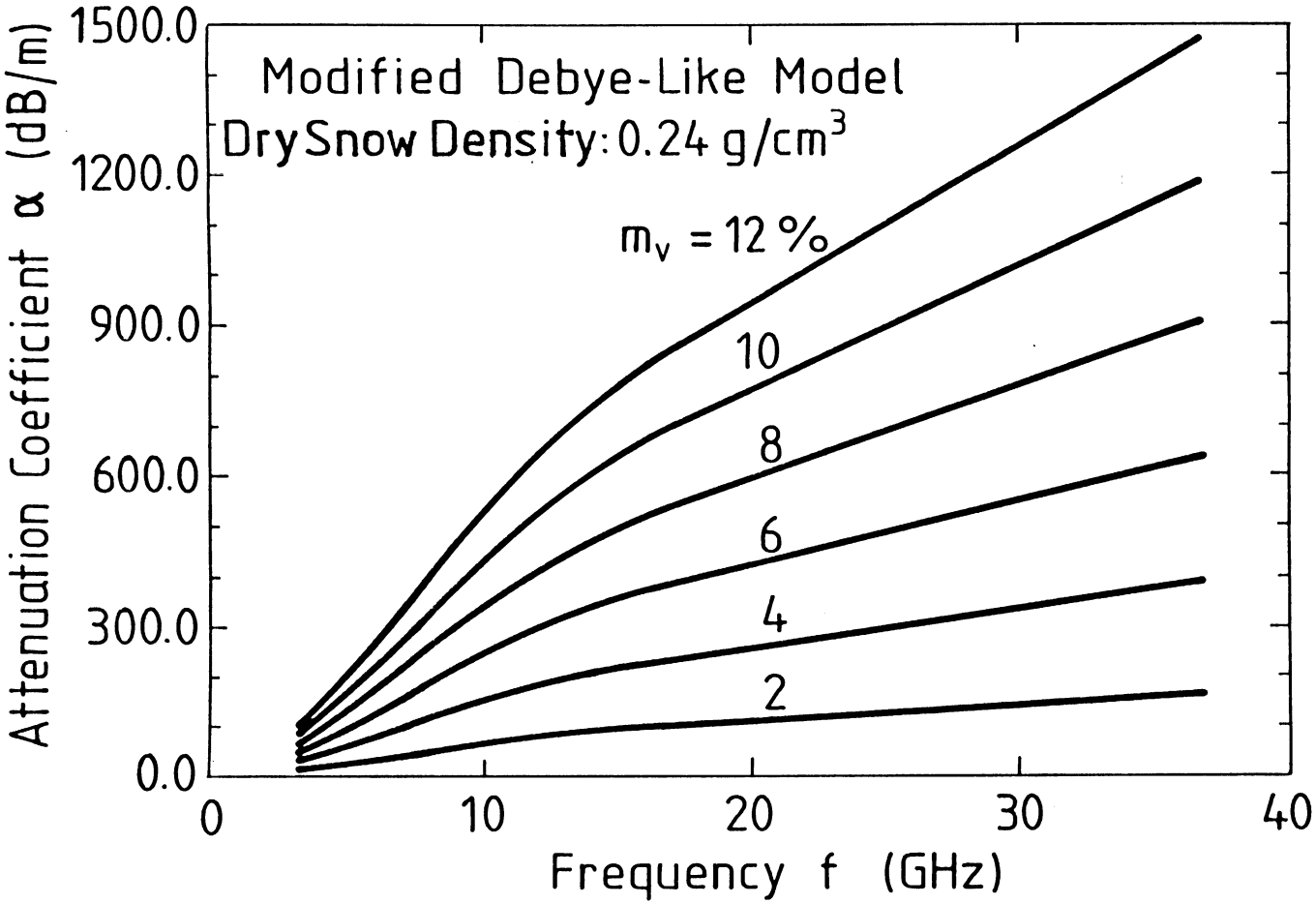

Hallikainen, Ulaby, Abdelrazi
Figure 15

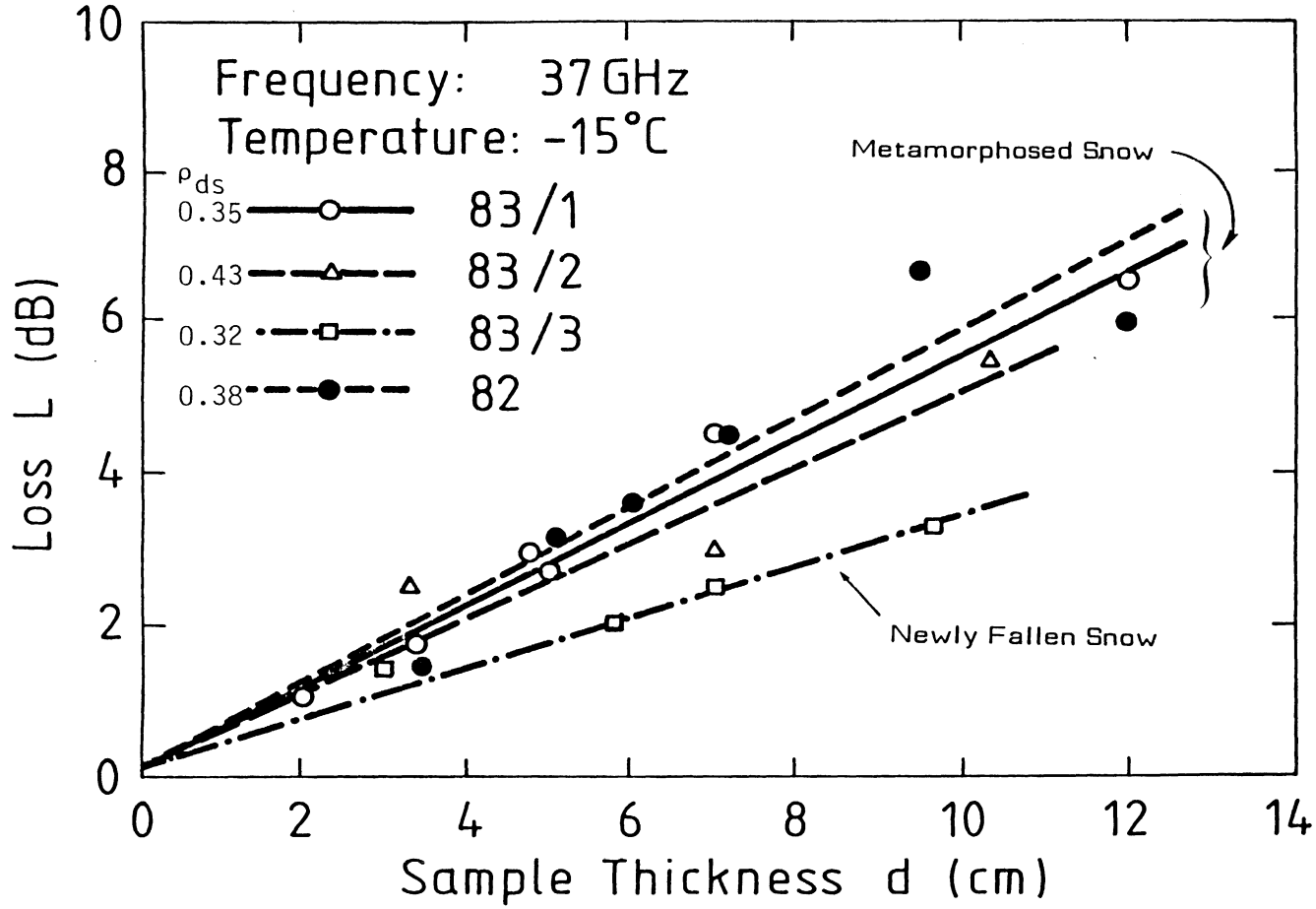

Hallikainen, Ulaby, Abdelrazik
Figure 16